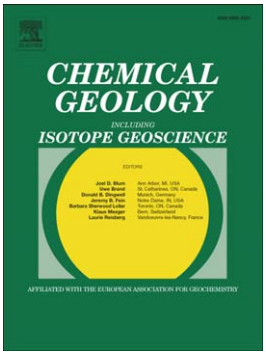

Reprint of Silicate-sulfide liquid immiscibility in modern arc basalt (Tolbachik volcano, Kamchatka): Part II. Composition, liquidus assemblage and fractionation of the silicate melt

Vadim S. Kamenetsky, Michael Zelenski, Andrey Gurenko, Maxim Portnyagin, Kathy Ehrig, Maya Kamenetsky, Tatiana Churikova, Sandrin Feig

PII: S0009-2541(17)30591-0
DOI: doi:10.1016/j.chemgeo.2017.10.026
Reference: CHEMGE 18515

To appear in: *Chemical Geology*

Received date: 25 February 2017
Revised date: 10 September 2017
Accepted date: 12 September 2017

Please cite this article as: Kamenetsky, Vadim S., Zelenski, Michael, Gurenko, Andrey, Portnyagin, Maxim, Ehrig, Kathy, Kamenetsky, Maya, Churikova, Tatiana, Feig, Sandrin, Reprint of Silicate-sulfide liquid immiscibility in modern arc basalt (Tolbachik volcano, Kamchatka): Part II. Composition, liquidus assemblage and fractionation of the silicate melt, *Chemical Geology* (2017), doi:10.1016/j.chemgeo.2017.10.026

Chemical Geology xxx (2017) xxx–xxx

Contents lists available at ScienceDirect

Chemical Geology

journal homepage: www.elsevier.com/locate/chemgeo

Reprint of Silicate-sulfide liquid immiscibility in modern arc basalt (Tolbachik volcano, Kamchatka): Part II. Composition, liquidus assemblage and fractionation of the silicate melt☆

Vadim S. Kamenetsky [a,b,*], Michael Zelenski [b], Andrey Gurenko [c], Maxim Portnyagin [d,e], Kathy Ehrig [f], Maya Kamenetsky [a], Tatiana Churikova [g], Sandrin Feig [h]

[a] CODES and Earth Sciences, University of Tasmania, Hobart, TAS 7001, Australia
[b] Institute of Experimental Mineralogy RAS, Chernogolovka 142432, Russia
[c] Centre de Recherches Pétrographiques et Géochimiques (CRPG), UMR 7358, Université de Lorraine, 54501 Vandoeuvre-lès-Nancy, France
[d] GEOMAR Helmholtz Centre for Ocean Research Kiel, 24148 Kiel, Germany
[e] V.I. Vernadsky Institute of Geochemistry and Analytical Chemistry, 119991 Moscow, Russia
[f] BHP Billiton Olympic Dam, Adelaide, SA 5000, Australia
[g] Institute of Volcanology and Seismology, Far East Branch, Russian Academy of Sciences, 683006 Petropavlovsk-Kamchatsky, Russia
[h] Central Science Laboratory, University of Tasmania, Hobart, TAS 7001, Australia

ARTICLE INFO

Article history:
Received 25 February 2017
Received in revised form 10 September 2017
Accepted 12 September 2017
Available online xxxx

Keywords:
Island arc
Magmatism
Sulfide melt
Volatiles
Immiscibility
Crystallization
Olivine
Melt inclusions

ABSTRACT

Olivine-hosted inclusions of silicate and sulfide melts, Cr-spinel and pyroxene were studied to estimate magma composition, temperature, pressure, and fO_2 at the onset and during the silicate-sulfide immiscibility in modern arc basalt from Tolbachik volcano, Kamchatka arc. We demonstrate that the olivine phenocrysts hosting sulfide and silicate melt inclusions belong to the same population. The compositions of the silicate melt inclusions in most primitive olivine (88–91 mol% Fo) represent moderately oxidized (~QFM + 1.1) high-MgO (up to 12–12.6 wt%) and high CaO/Al_2O_3 (0.8–1.2) melt that has abundances and ratios of the lithophile trace elements typical of island arc magmas. The initial volatile contents in parental Tolbachik magma are estimated from the melt inclusions and mass-balance considerations to be at least 4.9 wt% H_2O, 2600 ppm S, 1100 ppm Cl, 550 ppm F, and 1200 ppm CO_2. These data are used to calculate the temperature (~1220 °C) and minimum pressure (3 kbar) at which the beginning of crystallization and exsolution of sulfide melt took place. The presence of anhydrite, especially ubiquitous in the crystallized silicate melt associated with sulfide globules, suggest that much higher sulfur abundances prior to degassing and sulfate immiscibility and/or crystallization should be expected. We tentatively considered hydrothermal accumulations of sulfur (elemental, sulfate and sulfide) in the volcanic conduit responsible for local contamination and oversaturation of the Tolbachik magma in sulfur and related sulfide immiscibility. Coexisting sulfide and sulfate can be also interpreted in favor of the magmatic sulfide oxidation and related generation of S-rich fluids. Such fluids are expected to accumulate metals released from decomposed sulfide melts and supply significant epithermal mineralization, including native gold.

1. Introduction

The evolution of most mantle and crustal silicate magmas inevitably results in the separation of another phase of essentially non-silicate composition (e.g. Kamenetsky and Kamenetsky, 2010; Roedder, 1992). Such unmixing or immiscibility of two or more liquid and vapor phases occurs during continuously changing conditions associated with magma decompression, cooling, crystallization, mixing etc. The phenomenon of magmatic immiscibility in continental mafic magmas is most conspicuous for sulfide liquids that are commonly accepted as parental to Cu-Ni-PGE deposits, associated with komatiites, flood basalts and some layered intrusions (e.g. Naldrett, 2004). On the other hand, the origin of sulfide mineralization in subduction-related settings is still considerably debated. One possible explanation involves contribution of magmatic sulfides formed by unmixing of basaltic melts from earlier volcanic cycles. Several models imply genetic links between mineralizing fluids forming Cu-Au porphyry deposits to the silicate-sulfide liquid immiscibility in mafic magmas followed by breakdown of early-formed magmatic sulfides (e.g. Keith et al., 1997; Larocque et al., 2000; Wilkinson, 2013). Numerous experimental and theoretical

☆ A publishers' error resulted in this article appearing in the wrong issue. The article is reprinted here for the reader's convenience and for the continuity of the special issue. For citation purposes, please use the original publication details: Chemical Geology 471 (2017) 92-110.
DOI of original article: https://doi.org/10.1016/j.chemgeo.2017.09.019.

* Corresponding author at: School of Physical Sciences, University of Tasmania, Hobart, TAS 7001, Australia.
E-mail address: Dima.Kamenetsky@utas.edu.au (V.S. Kamenetsky).

https://doi.org/10.1016/j.chemgeo.2017.10.026
0009-2541/

studies defined favorable physical and chemical conditions for saturation in sulfide (e.g. Ariskin et al., 2013; Carroll and Rutherford, 1985; Fonseca et al., 2008; Haughton et al., 1974; Mavrogenes and O'Neill, 1999; Naldrett, 1969; O'Neill and Mavrogenes, 2002; Wohlgemuth-Ueberwasser et al., 2013). In particular, reduced conditions (i.e. low fO_2) were found beneficial to the appearance of immiscible sulfides even at low pressure (e.g. inclusions in glasses and olivine phenocrysts) in many primitive magmas (e.g. Gurenko et al., 1987; Kamenetsky and Kamenetsky, 2010), in particular at mid-ocean ridges (e.g. Ackermand et al., 2007; Francis, 1990; Kamenetsky et al., 2013; Mathez, 1976; Patten et al., 2012; Patten et al., 2013) and oceanic islands (e.g. Ackermand et al., 2007; Desborough et al., 1968; Skinner and Peck, 1969; Sobolev and Nikogosian, 1994; Stone and Fleet, 1991). In contrast, silicate-sulfide melt immiscibility is not routinely reported in basaltic magmas in the island arc setting because primitive arc basalts are much less common and generally more oxidized than continental and oceanic magmas (e.g. Brounce et al., 2014; Evans et al., 2012; Kelley and Cottrell, 2009; Kelley and Cottrell, 2012).

In general, records of immiscible phases in magmas have proved extremely difficult to document (Kamenetsky and Kamenetsky, 2010), largely because of their transient nature, small quantities and reactive qualities. In this study we employed recent discovery of abundant globules of Fe-Ni-Cu sulfide melt entrapped in high-Mg olivine (84–92 mol% Fo) in the lava and scoria of the 1941 eruption of the Tolbachik volcano, Kamchatka arc (Zelenski et al., 2017b, this volume). This extraordinary occurrence of coexisting immiscible liquids in the Tolbachik island-arc basalt provides an unparalleled opportunity to constrain the conditions of unmixing. Olivine-hosted inclusions, investigated in this study with a special emphasis on abundances and behavior of volatile elements, are used to estimate melt composition, temperature, pressure, and fO_2 at the onset and during the silicate-sulfide immiscibility. The parental melts are further explored for factors responsible for extensive unmixing of sulfide liquids.

2. Tolbachik volcano, 1941 CE eruption: a case of sulfide immiscibility

The Tolbachik volcanic massif is located southwest of the Klyuchevskoy Volcanic Group, which belongs to the northern part of the Kurile-Kamchatka arc almost at the Kamchatka-Aleutian arc junction. It is represented by two large stratovolcanoes, Ostry Tolbachik and Plosky Tolbachik (Fig. 1), that developed simultaneously during the Late Pleistocene (Braitseva et al., 1984; Churikova et al., 2015a; Ermakov and Vazheevskaya, 1973; Flerov et al., 2015). Since the beginning of the Holocene, volcanic activity related to a SW-NE fissure system developed through the summit of the Plosky Tolbachik volcano (Fig. 1). Several tens of monogenetic cinder cones, including those of three historical eruptions of 1941, 1975–1976 and 2012–2013, are apparently related to this fissure system (Fig. 1). Tolbachik rocks, where volatile, major and trace elements in melt inclusions in olivine were previously studied, are magnesian basalts of the Late Holocene cone "1004" (Portnyagin et al., 2007) and evolved basaltic andesites erupted in 2012–2013 (Plechov et al., 2015).

The 1941 eruption was the culmination of prolonged activity at the summit crater (including fumaroles and explosions in a lava lake at the bottom of the crater) which started in September 1939 and lasted for about 18 months (Piip, 1946). It occurred on the southern slope of Plosky Tolbachik at 1900 m a.s.l. approximately 4.5 km from the summit (3085 m a.s.l.). The eruption was very intensive – a scoria cone and 5 km of lava totaling ~0.1 km^3 formed during the first seven days (7–14 May 1939). At present, the 1941 eruption deposits are partially overlapped by products of the most recent (2012—2013) eruption.

In general, the Tolbachik magmas belong to two geochemical series with variable K_2O content at a given MgO (Churikova et al., 2015b). These series can be also distinguished in terms of other incompatible elements (e.g. P, Nb, Sr, Zr, rare-earths) and element ratios. Although both types of magmas contributed to the stratovolcano and monogenetic cones, it appears that the latter are dominated by high-K compositions.

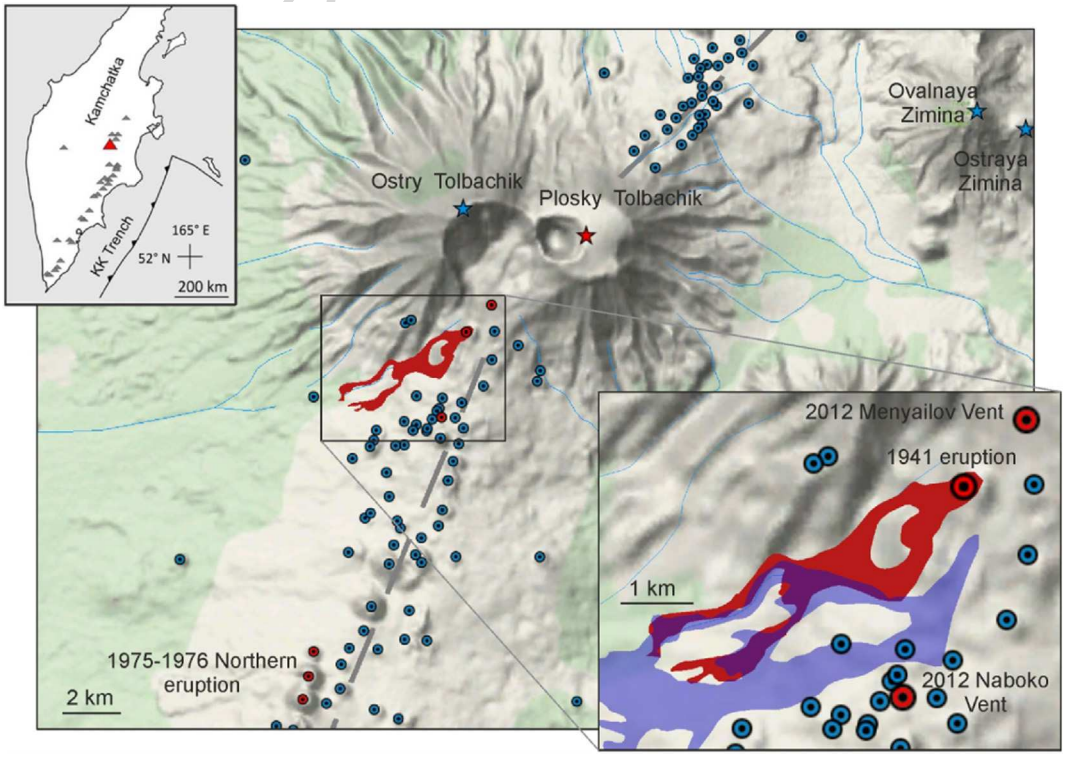

Fig. 1. Overview of the 1941 eruptive cone with adjacent lava (red field after Piip, 1946) situated at the SW slope of the Tolbachik volcanic massif. Red and blue stars show active and extinct volcanoes, respectively. The faults through the Plosky Tolbachik volcano (dashed lines) and location of pre-historic (blue circles) and historic (red circles) cinder cones are shown after Melekestsev et al., 1991). The 2012 Menyailov Vent lava shown in the inset as a purple field (after Gordeev et al., 2013) partly overlaps the products of the 1941 eruption. (For interpretation of the references to colour in this figure legend, the reader is referred to the web version of this article.)

Please cite this article as: Kamenetsky, V.S., et al., Reprint of Silicate-sulfide liquid immiscibility in modern arc basalt (Tolbachik volcano, Kamchatka): Part II. Composition, liquidus assemblage and ..., Chem. Geol. (2017), https://doi.org/10.1016/j.chemgeo.2017.10.026

The 1941 lava and scoria are high-K, moderately magnesian basalts (8.9% MgO, 9.7% FeO and Mg# 62–64, Supplementary Table S1), which belong to the intermediate group of Tolbachik rocks with $MgO/Al_2O_3 = 0.4–0.6$ and were interpreted as hybrid rock type produced by mixing of high-Mg middle-K and low-Mg high-K basalts (Portnyagin et al., 2015). In terms of Sr-Nd-Pb-O isotope ratios the 1941 eruption rocks fall within a very narrow range of Holocene Tolbachik rocks that suggests their origin from the same parental magma and much variability in trace elements generated by multi-cycle intracrustal fractionation (Portnyagin et al., 2015).

Sporadic (~2–4% of the rock) euhedral olivine, typically <1–5 mm in size, dominate the phenocryst assemblage, whereas pyroxene and Cr-spinel crystals are rare. The phenocrysts host abundant inclusions of silicate melt (glassy and crystallized), Cr-spinel, pyroxene, fluid and sulfide. The latter has been interpreted to result from silicate-sulfide immiscibility and described in detail in Zelenski et al. (2017b; this volume) and Zelenski et al. (2017a). A brief summary is presented below.

Approximately 0.6% of the total olivine population carry round and elliptical sulfide inclusions that vary in size from <1 μm to 250 μm. Sulfide inclusions in a given olivine phenocryst can occur as a single droplet, or most commonly several "scattered" globules of variable size, and rarely as "swarms" of several hundred spheres (Fig. 2a). Sulfide globules are associated with the silicate melt and magmatic fluid that occur as either individual inclusions in the same olivine grain or "coatings" around sulfides (Fig. 2b), or even captured inside sulfides (Fig. 2c). The sulfide droplets can also be components of multiphase inclusions containing a silicate melt, fluid bubble and crystals of clinopyroxene, orthopyroxene, Cr-spinel and anhydrite (Figs. 2b–f, 3). The sulfide globules have Fe-Ni-S compositions that can be variable in terms of Ni/Cu even within a single olivine host and olivine with the same Fo composition (Zelenski et al., 2017b, this volume).

3. Approach and analytical methods

Samples of lava and scoria from the 1941 Tolbachik eruption (Fig. 1b) were processed in a jaw crusher and sieved, followed by separation of olivine and clinopyroxene phenocrysts into a 0.5–1.5 mm

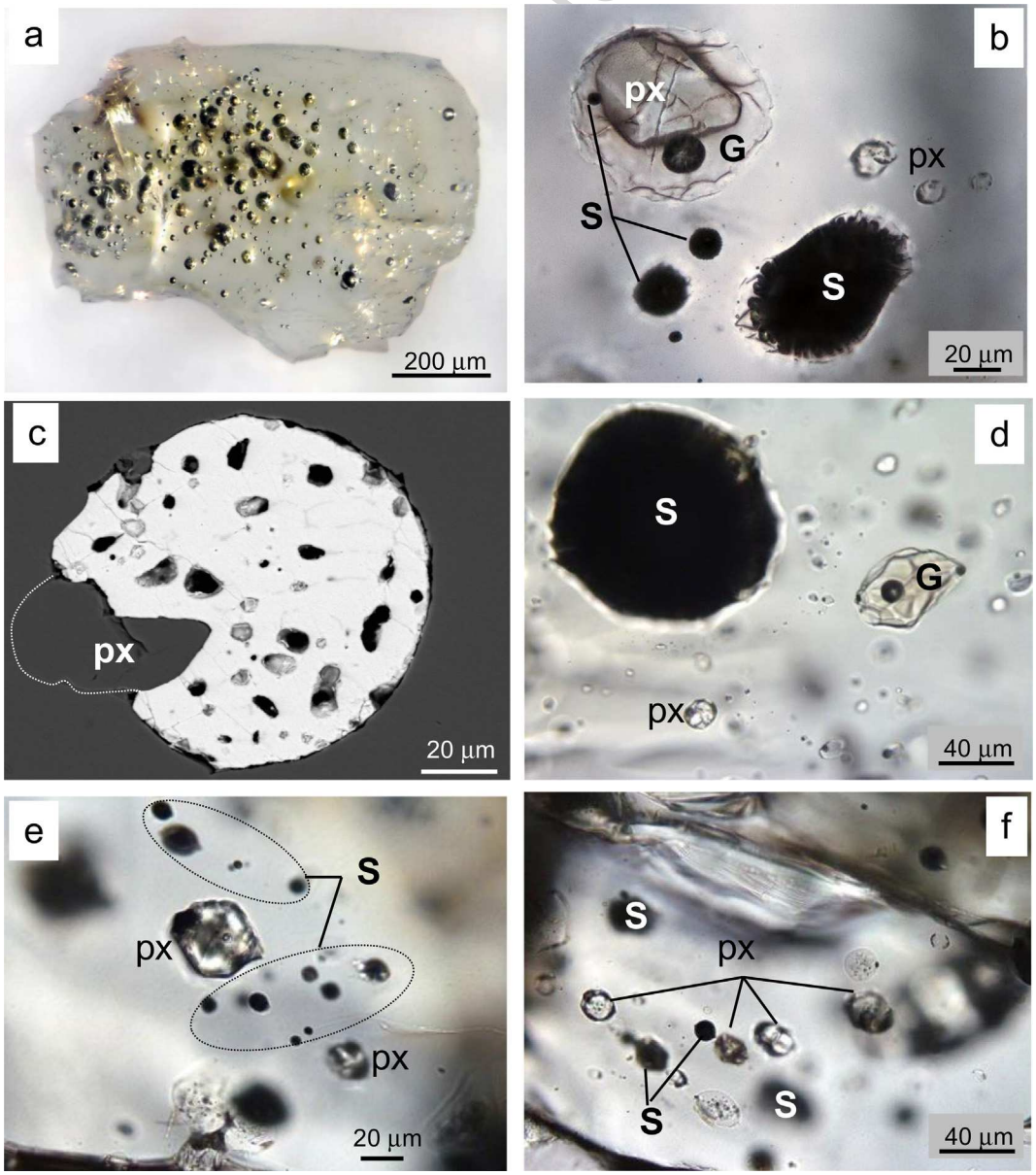

Fig. 2. Photomicrographs showing olivine-hosted inclusions of sulfide melt (S) coexisting with silicate glass (G) and clino- and orthopyroxene crystals (Px). Images are taken in reflected light (a), transmitted light (b, d–f) and backscattered electrons (c). Note vapor bubbles surrounding (b) and inside (c) sulfide globules.

Please cite this article as: Kamenetsky, V.S., et al., Reprint of Silicate-sulfide liquid immiscibility in modern arc basalt (Tolbachik volcano, Kamchatka): Part II. Composition, liquidus assemblage and ..., Chem. Geol. (2017), https://doi.org/10.1016/j.chemgeo.2017.10.026

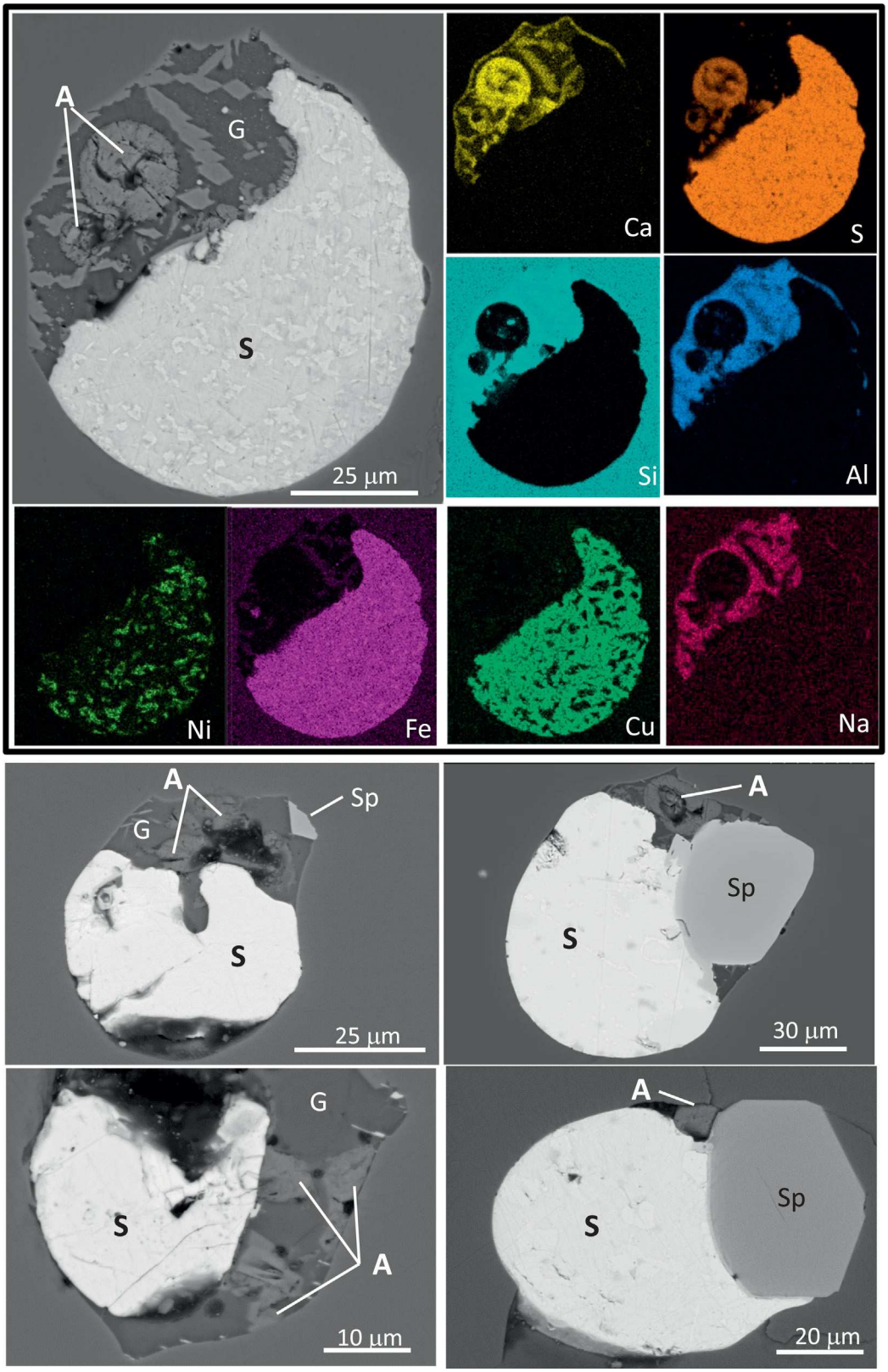

Fig. 3. Backscattered electron images and X-ray element maps of the olivine-hosted multiphase inclusions composed of large sulfide globules (S), silicate glass (G) with skeletal daughter clinopyroxene crystals, occasional Cr-spinel grains (Sp) and anhydrite droplets and crystals (A).

fraction using a heavy liquid and binocular microscope. Olivine crystals were then placed in a Petri dish and immersed in bromoform, a liquid with a high refractive index close to that of magnesian olivine (1.65–1.70), and examined for silicate and sulfide melt inclusions. Olivine grains containing a few inclusions of larger size (>50 μm) were preferentially picked by tweezers. Olivine grains from the lava samples, where melt inclusions commonly appear as crystalline aggregates, were wrapped in Pt foil with a piece of graphite, heated in a

Please cite this article as: Kamenetsky, V.S., et al., Reprint of Silicate-sulfide liquid immiscibility in modern arc basalt (Tolbachik volcano, Kamchatka): Part II. Composition, liquidus assemblage and ..., Chem. Geol. (2017), https://doi.org/10.1016/j.chemgeo.2017.10.026

vertical furnace at 1250 °C and 1 atm for 2 min, and then quenched in water. The experimental temperature was selected based on constraints by Portnyagin et al. (2015). Grains with homogenized melt inclusions and olivine from scoria with naturally quenched glassy inclusions (Fig. 2d) were mounted in epoxy resin and sequentially ground using a 1200 grit wet sandpaper. Grinding targeted large, homogeneous melt inclusions in central parts of the olivine grains. After such melt inclusions were exposed, their host grains were extracted, re-mounted and polished by 0.25 μm alumina powder for in-situ analysis by microbeam techniques.

The compositions of olivine, Cr-spinel and silicate melt inclusions were acquired in the Central Science Laboratory (University of Tasmania) by a Hitachi SU-70 Schottky field emission scanning electron microscope fitted with Oxford INCA Energy XMax 80 silicon drift detector energy dispersive system, followed by the quantitative analysis on a Cameca SX100 electron microprobe equipped with a tungsten filament and 5 wavelength dispersive spectrometers. To avoid damage, volatile loss and oxidation of glasses only one analytical spot in the center of each inclusion was performed. Major and trace element compositions of olivine and clinopyroxene phenocrysts, as well as olivine-hosted melt inclusions were analyzed using an Agilent 7500cs quadrupole ICP-MS with a 193 nm Coherent COMPex Pro ArF Excimer Laser at CODES Analytical Laboratories (University of Tasmania). Single analysis by LA-ICPMS of each inclusion-bearing olivine grain was done as close to glass/sulfide inclusions as possible. The volatile content of selected melt inclusions was determined by a CAMECA IMS 1270 E7 ion microprobe (CRPG, Nancy, France) using techniques described by Gurenko et al. (2016). Details of the analytical methods employed in this study are presented in Supplementary materials.

4. Results

4.1. Liquidus assemblage

The liquidus assemblage of the 1941 magma is dominated by phenocrystic olivine, whereas the amount of other crystals, such as clinopyroxene and Cr-spinel, is negligible. Importantly, clinopyroxene and Cr-spinel found as inclusions in olivine can be used to constrain the cotectic compositions. Sulfide globules found in some primitive olivine phenocrysts (85–92 mol% Fo, Figs. 4, 5; Table 1) suggest that the sulfide liquid was an intrinsic part of the magma at the very early stages of its evolution (Zelenski et al., 2017b, this volume), but likely disappeared from the liquidus of more evolved magmas, judging from strong (up to 300 ppm) Cu enrichment in low-Mg Tolbachik basalts (Portnyagin et al., 2015; Zelenski et al., 2016). However, the exact composition of the silicate melt undergoing sulfide immiscibility (the aim of this study) is not routinely obtained from melt inclusions coexisting with sulfide globules in the same olivine (Fig. 2b, d). First of all, silicate melt inclusions with the required size are rare and usually heterogeneous. Secondly, exposing them for in-situ analyses without the sulfide globules being polished away is technically difficult. Thirdly, they may represent a conjugate, not parental, silicate liquid. Therefore, we used a more reliable approach of analyzing silicate melt inclusions that are not necessarily co-trapped with sulfide globules in same olivine crystals. In this case, the compositions of sulfide-bearing olivine and olivine with the studied melt inclusions were thoroughly compared.

4.1.1. Olivine

Olivine phenocrysts from the 1941 basalt, used in this study, are represented by crystals in tephra, sometimes with thin coating of brownish

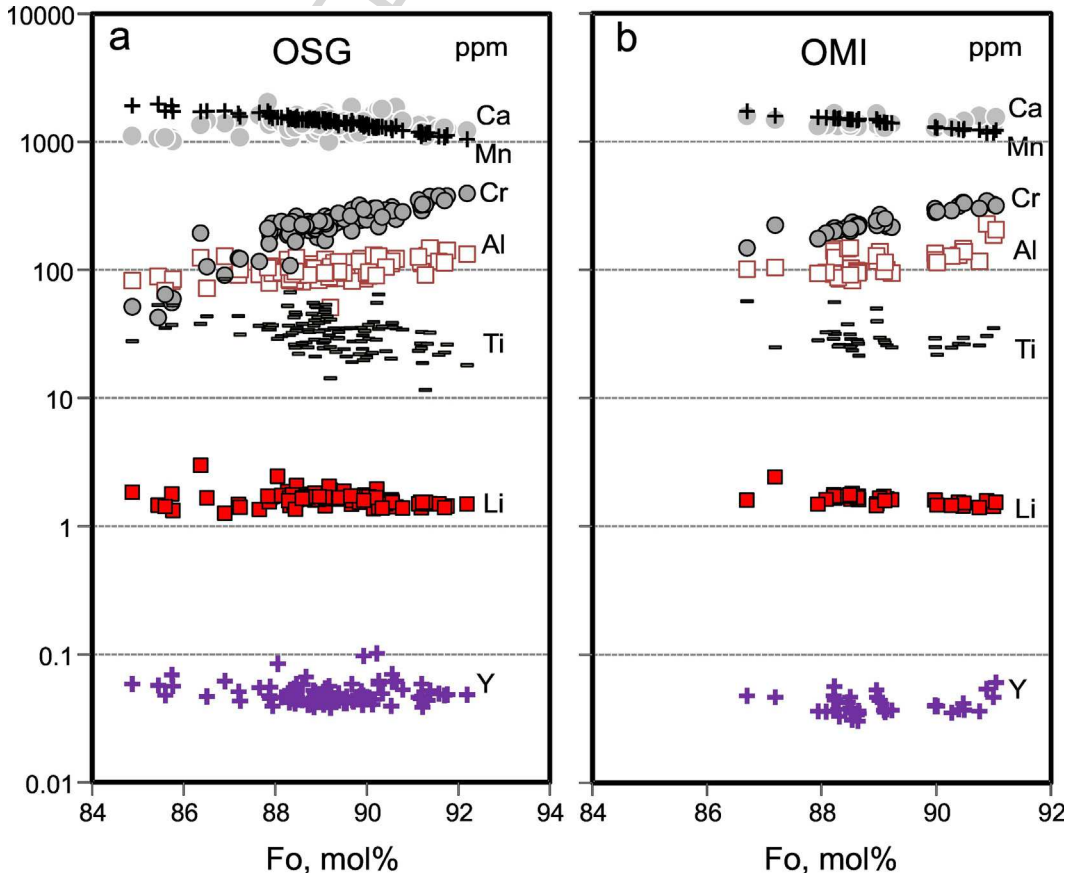

Fig. 4. Comparison of lithophile trace element compositions of olivine phenocrysts, containing sulfide globules (OSG) and silicate melt inclusions (OMI). Sizes of symbols on this and other figures are larger than analytical uncertainty.

Please cite this article as: Kamenetsky, V.S., et al., Reprint of Silicate-sulfide liquid immiscibility in modern arc basalt (Tolbachik volcano, Kamchatka): Part II. Composition, liquidus assemblage and ..., Chem. Geol. (2017), https://doi.org/10.1016/j.chemgeo.2017.10.026

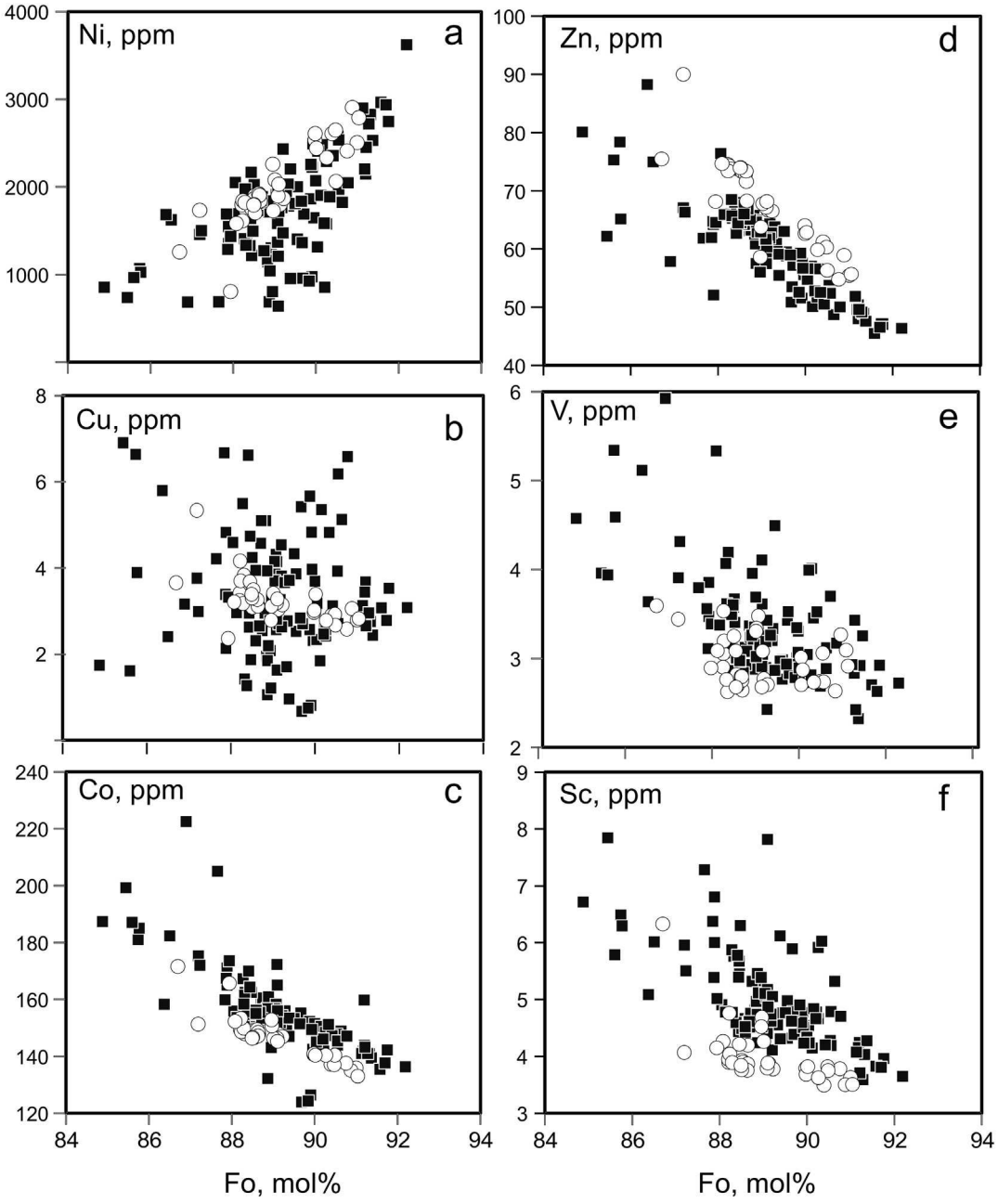

Fig. 5. Comparison of abundances of chalcophile trace elements and Sc in olivine phenocrysts, containing sulfide globules (OSG, *squares*) and silicate melt inclusions (OMI, *circles*).

glass attached to their surface, crystals in scoria bombs and from thick basalt lava. Most olivine crystals are unzoned or weakly zoned with Fe-rich thin rims and have compositions 80–92 mol% Fo, prevailed by values between 88 and 91 mol% (Figs. 4, 5). The olivine grains, belonging to different eruptive (magma fragmentation) modes, underwent cooling at different rates, from rapid (loose crystals) through intermediate (in tephra and bombs) to slow (lava flows). The cooling rate is reflected in the appearance of silicate melt inclusions that are predominantly glassy in olivine from tephra and partly- to fully crystalline in olivine from lavas and bombs.

The studied olivine phenocrysts can be tentatively subdivided into two types. Olivine containing silicate melt inclusions (hereafter, OMI) is prevailing, whereas grains with entrapped sulfide globules (hereafter, OSG) are <0.6% of the total olivine population. Trace element abundances and their relationships with major elements in olivine (Fo) are presented on Figs. 4, 5, Table 1 and Supplementary Table S2. It appears that OSG and OMI are similar in terms of Fo content (84–92 mol%), and are indistinguishable in terms of abundances of lithophile trace elements and their fractionation trends (Fig. 4). The trends, produced by increasing of Mn, Zn and V and decreasing Cr and Al with fractionation, are typical of olivine phenocrysts worldwide (e.g. Sobolev et al., 2007). However, the abundances of chalcophile elements (i.e. compatible with magmatic sulfides Ni, Co, Cu and Zn) and clinopyroxene-compatible Sc and V show notable differences between OSG and OMI (Fig. 5). Compatible in olivine Ni steadily decreases in OMI with olivine fractionation, however, its abundance in OSG is considerably scattered at a given Fo value, and systematically lower than those in OMI (Fig. 5a). Cobalt, Zn, V and Sc show incompatible behavior, so their contents in olivine increase with fractionation (Fig. 5c–f). Lithophile V and Sc appear to be consistently higher in OSG (Fig. 5e, f). Abundance of moderately chalcophile Co and Zn are systematically higher and lower, respectively, in OSG at a given Fo (Fig. 5c, d). Copper is almost

Please cite this article as: Kamenetsky, V.S., et al., Reprint of Silicate-sulfide liquid immiscibility in modern arc basalt (Tolbachik volcano, Kamchatka): Part II. Composition, liquidus assemblage and ..., Chem. Geol. (2017), https://doi.org/10.1016/j.chemgeo.2017.10.026

Table 1
Average forsterite (mol%) and trace element (ppm) composition of olivine phenocrysts hosting silicate melt inclusions (OMI) and sulfide globules (OSG).

	OMI		OSG	
	Aver	Std dev	Aver	Std dev
Fo	89.05	1.06	88.98	1.69
Li	1.64	0.17	1.65	0.21
Al	121	35	100	16
Ca	1388	105	1380	176
Sc	3.99	0.49	5.05	0.95
Ti	30.9	9.0	34.2	11.4
V	2.96	0.28	3.37	0.67
Cr	243	49	229	73
Mn	1421	131	1458	204
Co	147	7	156	15
Ni	1996	426	1721	569
Cu	3.23	0.50	3.39	1.47
Zn	68.2	7.6	60.9	9.0
Y	0.041	0.007	0.050	0.012
Yb	0.014	0.003	0.019	0.005

constant over the range of Fo in OMI (3.2 ± 0.5 ppm), whereas OSG have highly variable Cu contents (0.7–6.6 ppm; Fig. 5b) at a given Fo.

4.1.2. Cr-spinel and clinopyroxene

Cr-spinel occurs as reddish-brown euhedral to subrounded crystals, up to 60 μm across, included in olivine and olivine-hosted melt inclusions. Rarely, it can be found as swarms of blebby and dumbbell-shaped grains in association with sulfide droplets. Cr-spinel inclusions analyzed in the most primitive olivine (89–91 mol% Fo) are surprisingly variable in composition (Supplementary Table S3). The compositions differ in Cr_2O_3, Al_2O_3 and TiO_2 abundances and classified respectively as low-Al, high-Ti (average 15.0 and 0.66 wt%, respectively) and high-Al, low-Ti groups (average 12.0 and 0.49 wt%, respectively). Both compositional clusters are within the field of Cr-spinel compositions from calc-alkaline island arc rocks (Kamenetsky et al., 2001). All compositions are moderately oxidized ($Fe^{2+}/Fe^{3+} = 1.9–2.3$), could crystallize at ΔQFM = 1.1–1.34 (5–7 kbar, 1170 °C) as estimated following approach from Ballhaus et al. (1991) and in this respect correspond to those in basalts from oceanic islands and island-arcs (e.g. Evans et al., 2012; Kamenetsky et al., 2001). The temperatures of olivine – spinel equilibria estimated with the help of Al-in-olivine thermometer (Wan et al., 2008), except one point, range from 1139 to 1189 °C for host olivine $Fo_{89.9–89.3}$.

Clinopyroxene in the 1941 Tolbachik basalt is present as rare phenocrysts and common inclusions in olivine (Fig. 2). Although the clinopyroxene inclusions in primitive olivine (>89 mol% Fo) testify to early cotectic crystallization, the analyzed phenocrysts of clinopyroxene are much more evolved in terms of Mg# (molar ratio of $100 * Mg/(Mg + Fe^{2+})$, total Fe calculated as Fe^{2+}) than olivine in the same rocks. The majority of analyses demonstrate the range Mg# between 75 and 86 mol% (Fig. 6, Supplementary Table S3), whereas only one primitive clinopyroxene phenocryst (Mg# = 89.3) is found to match the average Fo content of olivine (89.0 mol%). Most minor and race elements in the clinopyroxene phenocrysts increase with decreasing Mg#, except Cr and Ni (Fig. 6d). However, only Al and Ga are well correlated with Mg# ($r^2 = 0.87$; Fig. 6a, c). All other elements, including clinopyroxene-compatible Cr and Sc, are scattered, sometimes significantly, at a given Mg#. The highest variations are recorded for crystals that have the most common composition of Mg# 78–80 mol%; for example, 1.1–2.2 ppm Yb, 11.3–23.1 ppm Y, 2.0–4.8 ppm Gd, 8–45 ppm Zr, 2.0–7.1 ppm Ce, etc. (Fig. 6b, e–g). On the other hand, in this dataset trace elements of similar and different incompatibility are well correlated, so the compositions, normalized to the primitive mantle (PM after Sun and McDonough, 1989), display essentially sub-parallel patterns (Fig. 6h). The PM-normalized compositions are typical of magmatic clinopyroxene in the island-arc settings in having concave downward patterns (maximum at Sm) with slightly negative Eu anomalies (Fig. 6h).

4.2. Melt inclusions

4.2.1. Appearance and phase composition

Olivine phenocrysts contain numerous primary melt inclusions (MI), typically spherical and ellipsoidal with variable wall faceting, 20–100 μm in size, rarely up to 300 μm. Naturally quenched MI from scoria and bombs are represented by brownish glass and a fluid bubble (Fig. 2d). Daughter crystals (i.e. crystallized in-situ) are not common, but clinopyroxene, Cr-spinel and sulfide globules of variable size can be occasionally co-trapped with the melt (Fig. 2b). The appearance of MI in olivine from the lava samples as semi-opaque aggregates of crystals reflects slower cooling and related crystallization of skeletal pyroxene, amphibole, Fe-Ti oxides and sulfide, set in the interstitial glass with fluid bubble(s). The crystalline inclusions in this study were heated to 1250 °C, homogenized and quenched to produce homogeneous glass for subsequent analyses.

Some partly crystalline MI contain varying amounts of anhydrite, represented by numerous small beads (<1 μm) scattered together with acicular clinopyroxene crystals in the glass. Larger-sized (up to 20 μm) porous aggregates and rarely well-shaped crystals are commonly recorded in multiphase inclusions with accidently trapped Cr-spinel and/or sulfide globule (Fig. 3). Anhydrite aggregates may occupy up to 20% of the inclusions' volume and appear to be "squeezed" in between the neighboring phases (i.e. host olivine and accidently trapped sulfide and Cr-spinel, Fig. 3). Anhydrite is only found inside partially crystallized MI, usually in association with sulfide globules (Fig. 3), but never as inclusions in olivine or a groundmass phase.

4.2.2. Chemical composition: major, trace and volatile elements

Both glassy and initially crystalline and then homogenized melt inclusions (hereafter, GMI and CMI, respectively) have FeO contents (6.7–9.8 wt%) negatively correlated with the Fo values of the host olivine (86.7–91.7 and 82.6–91.7 mol%, respectively). Thus, the MI in more primitive olivine suffered the so called "Fe-loss", caused by post-entrapment crystallization and re-equilibration with the host olivine (Danyushevsky et al., 2002). Consequently, measured glass compositions were first corrected to account for the Fe-loss (Danyushevsky et al., 2000) and then recalculated to match equilibrium with the host olivine using the Petrolog3 software (Danyushevsky and Plechov, 2011) and the model of Danyushevsky (2001) for water-bearing melts. The initial FeOt in all melt inclusions was assumed to equal 9.3 wt% (average for high-Mg Tolbachik basalts, Portnyagin et al., 2015), and Fe oxidation state was calculated following Kress and Carmichael (1988) at QFM + 1.1, deduced from the coexisting olivine and Cr-spinel compositions assuming the melts were saturated in orthopyroxene (see pyroxene inclusions in olivine in Fig. 2b–f). The above calculation was also based on assumptions that host olivine grains belong to the same fractionation trend (supported by trace element systematics on Fig. 4) and Fo values were not affected by possible fluctuations in fO_2 at given MgO and FeO contents in parental melts.

The melt compositions, corrected for in-situ olivine crystallization, for the majority of the studied MI in olivine >88 mol% Fo, are more primitive than those of the host magma and even the most magnesian rocks of Tolbachik (8.6–12.6, 8.9 and 10.7 wt% MgO, respectively; Figs. 7, 8; Supplementary Table S5). No principal differences in major element compositions of GMI and CMI at a given Fo are found in this study (Figs. 7, 8). A striking feature of all the melt inclusions is their high and variable CaO/Al_2O_3 values (0.72–1.2, average 0.95) that are significantly higher than those in the 1941 rocks (0.67) and the majority of other Tolbachik magmas except for the most high-Mg basalts with CaO/Al_2O_3 approaching 0.85 (Fig. 7). The high CaO/Al_2O_3 in MI appear to be a consequence of both elevated CaO (12–15 wt%) and low Al_2O_3

Please cite this article as: Kamenetsky, V.S., et al., Reprint of Silicate-sulfide liquid immiscibility in modern arc basalt (Tolbachik volcano, Kamchatka): Part II. Composition, liquidus assemblage and ..., Chem. Geol. (2017), https://doi.org/10.1016/j.chemgeo.2017.10.026

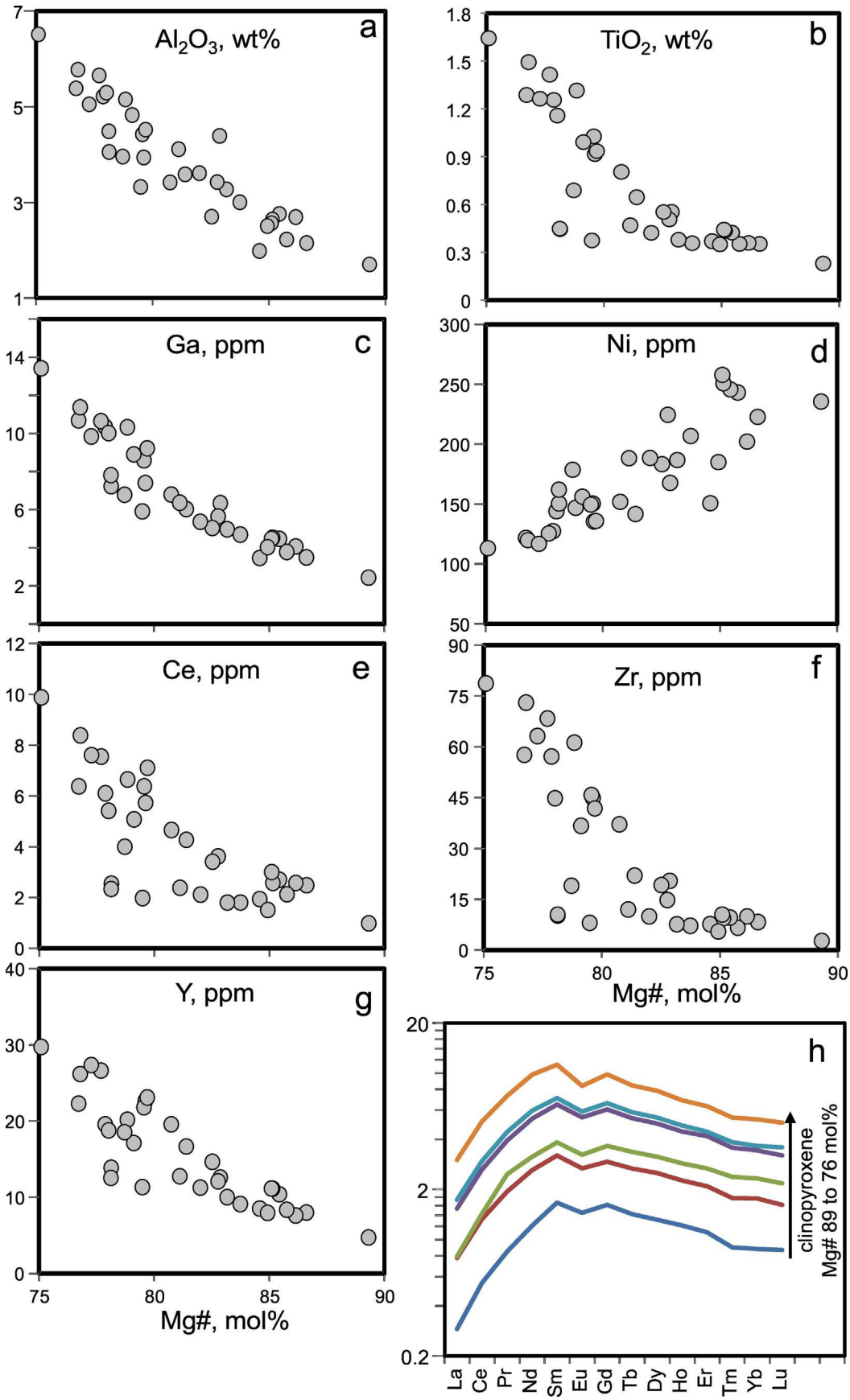

Fig. 6. Major and trace element compositions of clinopyroxene phenocrysts. Primitive mantle-normalized (after Sun and McDonough, 1989) rare earth element compositions are presented on (h).

Please cite this article as: Kamenetsky, V.S., et al., Reprint of Silicate-sulfide liquid immiscibility in modern arc basalt (Tolbachik volcano, Kamchatka): Part II. Composition, liquidus assemblage and ..., Chem. Geol. (2017), https://doi.org/10.1016/j.chemgeo.2017.10.026

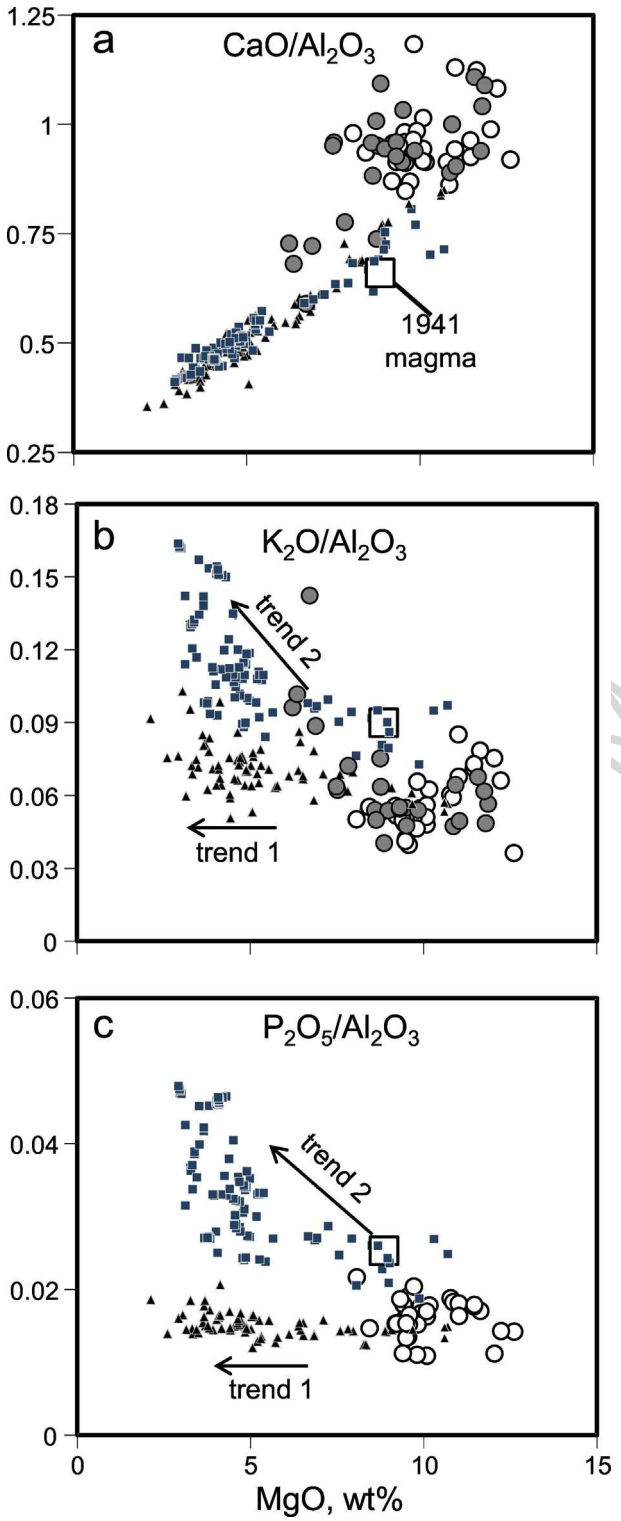

Fig. 7. Comparison between compositions (element ratios) of Tolbachik rocks and olivine-hosted melt inclusions from the 1941 eruption. Rocks are represented by middle-K (*triangles*) and high-K (*squares*) series (Churikova et al., 2015a, 2015b; Portnyagin et al., 2015). Average 1941 rock is shown by large square (Supplementary Table S1). Melt inclusions are naturally glassy (GMI, *open circles*) and initially crystalline and then homogenized (CMI, *filled circles*). All melt inclusion compositions are recalculated to be in equilibrium with host olivine (Supplementary Table S5).

(12–14 wt%) contents (Fig. 8). CaO contents increase from ~12 wt% with olivine fractionation and reach maximum values at ~8 wt% MgO (~88 mol% Fo), and then steadily decrease in both MI and rock compositions (Fig. 8c), thus reflecting a dominant control from crystallizing clinopyroxene. Similar to CaO, the CaO/Al_2O_3 values, as well as the other elements normalized to Al_2O_3, are significantly scattered in MI hosted by primitive olivine (>88 mol% Fo; Fig. 7).

The major and trace element compositions of MI (Figs. 8–10; Supplementary Table S5) appear to be consistent with the Tolbachik whole-rock compositions but extend to higher MgO and lower concentrations of elements that are incompatible in olivine. The contents of most elements in MI (e.g. Ti, Al, Na and incompatible elements like K and P; Fig. 8) are broadly correlated with the degree of crystal fractionation, showing increase with decreasing MgO, and, to some extent, they fit the whole-rock compositional trends (discussed below). The MI in the most primitive olivine 90–91 mol% Fo have variable, though generally high K_2O abundances (0.45–1.05 wt%, Fig. 9), which do not correlate with CaO/Al_2O_3 or other major elements. The K_2O contents in MI in less primitive olivine (88–91 mol% Fo) remain variable and unchanged, but increase abruptly towards those in the 1941 Tolbachik magma (1.3 wt%) in the most evolved MI in this study (<85 mol% Fo).

Incompatible trace element abundances and trace element ratios (e.g. light to heavy rare-earth elements, LREE/HREE) in MI are also highly variable. Light and middle REE (La to Gd), large-ion lithophile elements (Rb, Sr), Th, U and B correlate well with K_2O and each other, and make a trend towards the 1941 magma composition (Fig. 9). No significant correlations are observed between K_2O and more compatible heavy REE, high-field strength elements (Ti, Nb, Ta, Zr and Hf), Ba and Pb. The patterns of the PM-normalized trace-element abundance have well-developed depletions in HFSE and Th, whereas, LILE, U and Pb are markedly enriched relative to REE of similar incompatibility (Fig. 10). These specific enrichments and depletions, also shared by the Tolbachik rocks, are typical of subduction zone magmas. They are widely attributed to the selective addition of LILE > LREE > HFSE by melt and/or fluid derived from subducting oceanic crust (e.g. Arculus and Johnson, 1981; McCulloch and Gamble, 1991; Perfit et al., 1980) and are not discussed henceforth. Quantitative modelling of incompatible trace element composition in parental Tolbachik magmas was recently presented by Portnyagin et al. (2015).

The contents of volatile elements (S, Cl, F) in GMI and CMI were analyzed by the electron and ion microprobes (Table 2). The data presented below were obtained by the ion microprobe (SIMS) and include H_2O abundances measured in the same MI by the same method together with other volatiles (Figs. 11, 12). The analyzed MI represent a broad range of melt compositions (Fig. 11), entrapped in primitive olivine $Fo_{84–91}$. The GMI analyzed for volatiles have statistically higher H_2O (3.8–5.3 wt%), Cl (1050–1390 ppm) and S (2460–3900 ppm) than the CMI (0.6–4.3 wt% H_2O, 620–1450 ppm Cl, 840–2850 ppm S; Table 2, Fig. 11). No significant differences are observed for fluorine content in GMI and CMI (555 ± 54 ppm and 529 ± 88 ppm, respectively; Table 2). Sulfur abundances in both GMI and CMI are positively correlated with H_2O and Cl contents (Fig. 11e, f), whereas neither CO_2 nor F concentrations show any correspondence to other volatile elements (Table 2).

5. Discussion

Ubiquitous sulfide globules entrapped in primitive olivine phenocrysts of the 1941 Tolbachik eruption may provide a new perspective on several key outstanding problems in understanding silicate-sulfide immiscibility in primitive island-arc magmas. We further tackle this conundrum by placing better constraints on natural factors that potentially control magma unmixing, such as parental melt composition, temperature, pressure and oxygen fugacity. In this study all these important chemical and physical parameters are inferred from crystal and silicate melt inclusions in olivine phenocrysts (OMI). However, the applicability of these factors to processes responsible for immiscible sulfide globules in olivine phenocrysts (OSG) needs to be additionally discussed by comparing OMI and OSG.

Please cite this article as: Kamenetsky, V.S., et al., Reprint of Silicate-sulfide liquid immiscibility in modern arc basalt (Tolbachik volcano, Kamchatka): Part II. Composition, liquidus assemblage and ..., Chem. Geol. (2017), https://doi.org/10.1016/j.chemgeo.2017.10.026

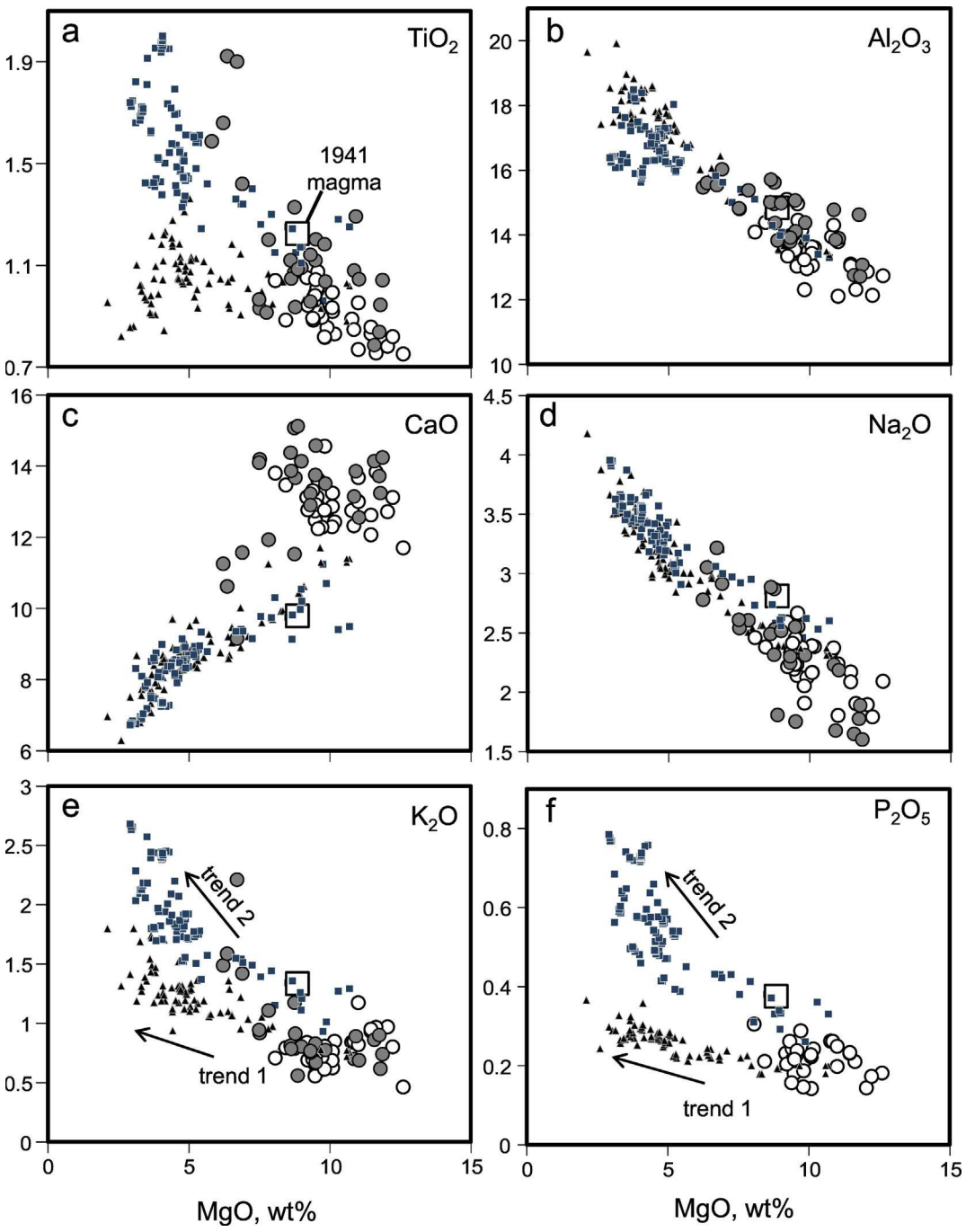

Fig. 8. Comparison between major element compositions of Tolbachik rocks and olivine-hosted melt inclusions from the 1941 eruption. Rocks are represented by middle-K (*triangles*) and high-K (*squares*) series (Churikova et al., 2015a, 2015b; Portnyagin et al., 2015). Average 1941 rock is shown by large square (Supplementary Table S1). Melt inclusions are naturally glassy (GMI, *open circles*) and initially crystalline and then homogenized (CMI, *filled circles*). All melt inclusion compositions are recalculated to be in equilibrium with host olivine (Supplementary Table S5).

5.1. Do olivine phenocrysts belong to a single population?

Below we consider whether the olivine phenocrysts containing the studied silicate melt inclusions (OMI) are genetically related to olivine grains bearing sulfide globules (OSG). First of all, both olivine types belong to the same eruption, i.e. were transported to the surface by the same magma batch. Secondly, they belong to the same stage of magma fractionation, and most likely to same temperature interval, as evidenced by their overlapping major element compositions (84–92 mol% Fo; Figs. 4, 5, Table 1). Importantly, the compositions of OSG and OMI are indistinguishable in terms of abundances of lithophile trace elements and their relationships with Fo content (e.g. fractionation trends, Fig. 4). In contract, the systematics of certain chalcophile elements shows differences between olivine containing silicate melt inclusions and sulfide globules. For example, Ni and Zn abundances in OSG are systematically lower than those in OMI and scattered at a given Fo (Fig. 5a, d); this can be confidently assigned to partitioning of these elements into the sulfide melt at the time of olivine crystallization. On the other hand, Co that is supposedly a chalcophile element demonstrates a steady fractionation trend and marginally higher abundances in OSG than in OMI (Fig. 5c, Table 1). Copper abundances, significantly scattered in OSG compared to those in OMI (Fig. 5b, Table 1), most likely reflect processes associated with sulfide immiscibility, both as Cu addition by a fluid to a given parcel

Please cite this article as: Kamenetsky, V.S., et al., Reprint of Silicate-sulfide liquid immiscibility in modern arc basalt (Tolbachik volcano, Kamchatka): Part II. Composition, liquidus assemblage and ..., Chem. Geol. (2017), https://doi.org/10.1016/j.chemgeo.2017.10.026

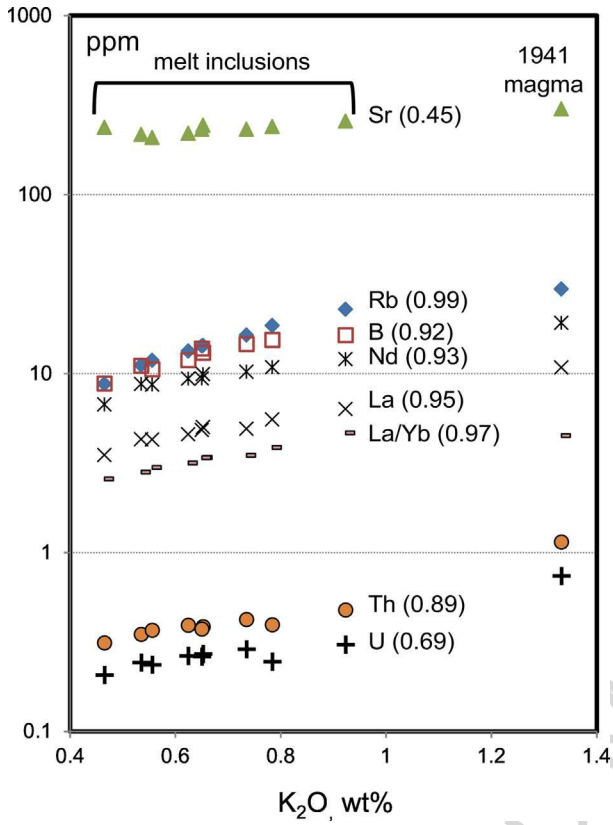

Fig. 9. Variability and covariation of incompatible trace elements with K_2O in glassy melt inclusions (GMI) and average 1941 rocks (Supplementary Table S1). Numbers in parentheses show r^2 coefficient of determination for linear regression for the melt inclusions data.

of melt (Kamenetsky and Kamenetsky, 2010; Kamenetsky and Eggins, 2012) and/or Cu extraction by the immiscible sulfide melt. Thus, the Cu contents of the melt undergoing sulfide immiscibility appears as highly variable (~25 to 235 ppm Cu), based on 0.7–6.6 ppm Cu in OSG (Fig. 5c) and partitioning of Cu between olivine and melt (D_{Cu} = 0.028 according to Portnyagin et al., 2017). In contract, the almost constant Cu contents in OMI (3.2 ± 0.5 ppm) over the range of Fo correspond to Cu in the melt of 114 ± 17 ppm, which is similar to that in the melt inclusions (Supplementary Table S6). Systematically higher V contents in OSG (Fig. 5e) provide support for locally reducing conditions (e.g. Canil and Fedortchouk, 2000; Lee et al., 2005) that were instrumental in causing sulfide saturation. Finally, the clinopyroxene-compatible Sc is significantly higher in OSG than in OMI (Fig. 5f, Table 1), however, this is not fully understood, given a steady association of clinopyroxene inclusions and sulfide globules in OSG (Fig. 2).

In conclusion, we are confident that both types of olivine represent the same batch of magma, where the sulfide saturation was locally achieved, thus affecting some compositional characteristics of olivine phenocrysts containing sulfide globules. Therefore, the constraints presented below are based upon the assumption that the studied silicate melt inclusions exemplify an island-arc magma on the brink of sulfide saturation.

5.2. Melt compositions: melt inclusions vs whole rocks

The composition of the melt undergoing sulfide immiscibility is not only important in terms of the sulfide-forming Fe^{2+} and S^{2-}, but it provides a cornerstone upon which assessment of other parameters is based. For example, calculations of temperature depend on the melt's MgO and H_2O contents, whereas pressure estimates are derived from abundances of soluble volatiles. The possible uncertainty in the estimated fO_2 of an order of magnitude introduces the uncertainty of ~1 wt% MgO to the reconstructed composition of melt inclusions. This compositional shift is relatively small compared to the large range of MI compositions and does not affect conclusions of this study. Thus, we are only concerned whether the melt inclusions in this study are related to magmas that formed Tolbachik rocks.

The incompatible trace-element geochemistry and the phenocryst assemblage and chemistry of the 1941 Tolbachik melt inclusions (Fig. 10) are characteristic of subduction zone magmas *sensu stricto*. High-Mg compositions of the Tolbachik olivine phenocrysts (88–91 mol% in the majority of crystals) point to the primitive nature of their parental magmas. Importantly, the melt inclusions trapped in such magnesian olivine suggest significant compositional heterogeneity in both major and trace element abundances (Figs. 7–9). For example, a range of TiO_2 and Al_2O_3 contents in most primitive melt inclusions (Fig. 8a, b) is independently confirmed by varying concentrations of TiO_2 and Al_2O_3 in the melts in equilibrium with the Cr-spinel (0.7–1.0 wt% and 11.5–13.5 wt%, respectively; calculated using the empirical model by Kamenetsky et al., 2001. The compositional diversity of the most primitive melts is also reflected in variability of the incompatible lithophile elements (Figs. 9, 10a) that are generally decoupled from the major elements (except K_2O).

The compositions of relatively evolved melt inclusions and primitive Tolbachik rocks largely overlap (Figs. 7, 8). The compositional heterogeneity demonstrated by the melt inclusions is also pronounced in the Tolbachik magmas and even enhanced towards more evolved compositions (<5 wt% MgO). The variations in K_2O content at a given MgO (Fig. 8e) have been previously assigned to two series, middle-K and high-K, or trend 1 and trend 2, respectively, depicting co-variations of K_2O and MgO (Churikova et al., 2015b). Similar distinct trends can be seen for other elements, e.g. Ti, Fe, P and incompatible trace elements. The separation between the trends is weak for Al and Na, and all Tolbachik rocks are indistinguishable in terms of their Ca systematics (Fig. 8c). The two trends are most spread out towards low MgO compositions, but they converge at the high-Mg end of the spectrum, where the Tolbachik basalts are seemingly merged with the compositions of the melt inclusions (Figs. 7, 8). Relatively evolved melt inclusions are compositionally similar to the 1941 Tolbachik magma (Figs. 7, 8), which belong to the high-K trend 2 (Churikova et al., 2015b). Similarly, there is strong resemblance between the trace element compositions of the melts parental to clinopyroxene phenocrysts, calculated using a set of partition coefficients (Hart and Dunn, 1993), and the 1941 Tolbachik magma (Fig. 10b). The geochemical systematics of the average primitive melt inclusion can be related to those of the host magma by ~50% fractionation (Fig. 10b), however, the decreased Sr/Nd and increased Zr(Hf)/Sm and Nb(Ta)/La ratios in the plagioclase-free 1941 rock cannot be explained by simple fractional crystallization model.

Widespread mixing processes of evolved and primitive magmas under the Tolbachik volcanic field were proposed for trend 2 in recent Tolbachik rocks (Portnyagin et al., 2015). In detail, using major and trace elements the authors quantitatively demonstrated that the series of recent Tolbachik magmas trending towards high-K compositions corresponds closely to the expected range of magmas potentially generated in long-lived shallow fractionating magma chamber, which is open for periodic eruptions and replenishments by more primitive magma (Lee et al., 2014; O'Hara, 1977; O'Hara and Mathews, 1981). In contrast, the trend 1 of Churikova et al. (2015b), which is typical for rocks of older and presently inactive Ostry Tolbachik volcano, can be explained by simple fractional crystallization model of the same parental magma. Melt inclusions studied here overlap both rock trends in high-MgO compositional field and thus can be interpreted as a snapshot of highly heterogeneous Tolbachik plumbing system, comprising batches of magmas formed either by fractional crystallization of more primitive magmas or by mixing of primitive medium-K and evolved high-K melts. As high-K melt inclusions were found in high-Fo olivine, it is

Please cite this article as: Kamenetsky, V.S., et al., Reprint of Silicate-sulfide liquid immiscibility in modern arc basalt (Tolbachik volcano, Kamchatka): Part II. Composition, liquidus assemblage and ..., Chem. Geol. (2017), https://doi.org/10.1016/j.chemgeo.2017.10.026

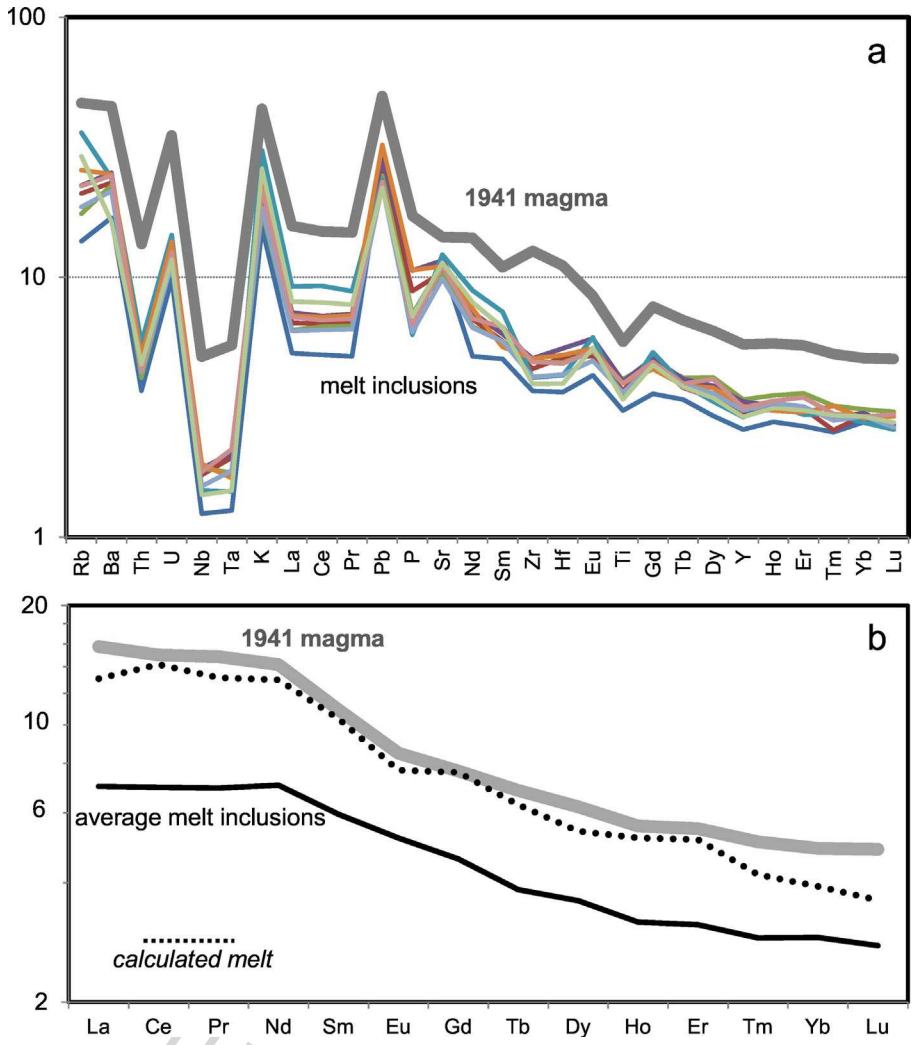

Fig. 10. Primitive mantle-normalized (after Sun and McDonough, 1989) lithophile trace element compositions of glassy melt inclusions (GMI) in comparison to average 1941 Tolbachik magma (a, b) and melt calculated in equilibrium with the average clinopyroxene composition (b).

plausible that magma mixing might affect the entire evolutional path of the Tolbachik magmas beginning from the very early stages of their crustal evolution. Notably, the model can consistently explain high K_2O as well as lower Sr/Nd, Nb/La, Ba/Rb and other geochemical features of the high-K inclusions as they contain significant fraction of a strongly evolved melt component, which composition reflects extensive multi-stage plagioclase and pyroxene crystallization. Increasingly large variability of trace elements in clinopyroxene phenocrysts with decreasing their Mg# suggests similar scenario of magma evolution when predominating incompatible trace element (e.g., Ce, Zr, Fig. 6) enriched pyroxenes crystallized from hybrid magmas and relatively depleted compositions crystallized from magmas fractionated in closed system.

Irrespective of fractionation factors responsible for the compositional trends demonstrated by rocks, the compositions of melt inclusions and clinopyroxene phenocrysts in this study (Figs. 6–10) strongly suggest large variability in parental Tolbachik melts. Among other parameters, variable and high CaO/Al_2O_3 ratios in the melt inclusions, especially when compared to those in the whole rocks, are both puzzling and potentially significant for understanding silicate-sulfide immiscibility.

5.3. Possible origins of high-Ca melts

A distinctive feature of the studied melt inclusions in the 1941 Tolbachik primitive olivine phenocrysts – high CaO/Al_2O_3 ratios (0.85–1.2) that reflect high CaO abundances (Fig. 8c), is not present in the host magma (0.67) and only marginally overlapping with CaO/Al_2O_3 in the most magnesian Tolbachik rocks (up to 0.85, Portnyagin et al., 2015). High-CaO, high CaO/Al_2O_3 melt inclusions are not common, but have been recorded in several studies of olivine-phyric lavas in island arcs and other geodynamic settings (e.g. Danyushevsky et al., 2004; de Hoog et al., 2001; Della-Pasqua and Varne, 1997; Elburg et al., 2006; Elburg et al., 2007; Gioncada et al., 1998; Kamenetsky et al., 1995a,b, 1997, 1998, 2006, 2007; Kamenetsky and Gurenko, 2007; Métrich et al., 1999; Portnyagin et al., 2005a; Schiano et al., 2000; Sorbadere et al., 2013). The high-CaO geochemical signature of olivine-hosted melt inclusions usually contrasts with those of bulk-rock and glass analyses, but in some cases primitive high-CaO magmas with unusual $CaO/Al_2O_3 > 1$ do occur in island arcs systems, mostly in the western Pacific, such as Kamchatka (Kamenetsky et al., 1995b; Portnyagin et al., 2005b), Vanuatu (Barsdell, 1988; Barsdell and Berry, 1990), Valu Fa Ridge, Lau Basin (Kamenetsky et al., 1997), the New Georgia Group of the Solomon Islands (Ramsay et al., 1984; Schuth et al., 2004) and Indonesia (Elburg et al., 2007; Foden, 1983). Many of these rocks are often strongly clinopyroxene-phyric (so called ankaramites), and thus some uncertainty surrounds whether their compositions are the product of clinopyroxene phenocryst accumulation or reflect significant clinopyroxene component in the composition of parental melts (Della-Pasqua and Varne, 1997).

Please cite this article as: Kamenetsky, V.S., et al., Reprint of Silicate-sulfide liquid immiscibility in modern arc basalt (Tolbachik volcano, Kamchatka): Part II. Composition, liquidus assemblage and ..., Chem. Geol. (2017), https://doi.org/10.1016/j.chemgeo.2017.10.026

Table 2
Major and volatile element compositions of olivine-hosted melt inclusions.

	Crystalline melt inclusions (CMI)												Glassy melt inclusions (GMI)												
Grain no	4	5	7	11	12	14a	14b	16	17a	17b	18a	18b	19	20	24	30	13	28a	30	31	38	59	73	75	79
D melt incl, μm	69	81	35	55	89	55	38	75	63	56	94	75	41	88	41	86	150	113	100	125	113	119	115	125	102
D bubble, μm	18	25	n.a.	16	22	n.a.	15	20	13	15	33	25	12	25	14	28	50	33	38	45	45	38	30	40	41
Volatiles by SIMS (CRPG, Nancy)																									
N repl	3(1)	3(3)	3(3)	3(2)	3(1)	3(1)	3(3)	3(3)	3(0)	3(3)	3(3)	2(1)	3(1)	3(1)	3(3)	3(3)	3(3)	3(2)	3(3)	3(1)	3(3)	3(3)	5(3)	3(3)	6(4)
CO_2, ppm	755	507	584	1134	551	648	807	939		565	1174	1031	972	864	687	54	782	598	906	730	862	834	1053	724	872
RSD, %	*0.2*	*2.2*	*13.4*	*0.8*	*4.1*	*1.3*	*1.5*	*2.1*	–	*8.9*	*3.4*	*2.1*	*6.8*	*1.3*	*14.7*	*3.5*	*3.7*	*1.5*	*7.4*	*0.2*	*1.4*	*8.6*	*14.7*	*2.6*	*7.0*
F, ppm	552	583	453	610	375	604	734	576	550	510	553	410	489	459	541	472	572	550	506	536	678	495	535	537	589
RSD, %	*8.5*	*1.4*	*2.5*	*7.2*	*3.4*	*15.1*	*9.6*	*1.3*	*4.7*	*1.4*	*7.0*	*4.1*	*2.3*	*10.4*	*7.0*	*3.6*	*1.9*	*3.9*	*2.6*	*3.9*	*6.2*	*1.9*	*6.0*	*1.7*	*3.4*
S, ppm	1979	2177	2465	2465	2203	2455	2848	1430	2002	843	2631	1623	1616	2714	2229	1072	2660	3385	2971	3137	2833	2790	2607	2786	2456
RSD, %	*12.1*	*1.3*	*3.6*	*6.2*	*6.4*	*10.6*	*5.5*	*1.3*	*3.9*	*0.3*	*4.2*	*2.5*	*1.8*	*7.8*	*6.2*	*2.9*	*3.5*	*2.8*	*0.7*	*6.3*	*4.9*	*2.9*	*3.5*	*0.7*	*2.2*
Cl, ppm	1026	1012	1196	862	1068	1285	1447	859	1038	617	1276	925	969	1263	1055	980	1173	1375	1289	1388	1196	1263	1234	1309	1048
RSD, %	*10.5*	*2.3*	*2.1*	*4.5*	*6.3*	*10.2*	*9.6*	*0.6*	*3.0*	*1.1*	*6.3*	*1.1*	*3.8*	*9.8*	*4.1*	*3.9*	*5.3*	*2.9*	*2.0*	*6.1*	*7.3*	*4.8*	*5.1*	*0.9*	*3.8*
H_2O, wt%	1.86	3.33	1.71	3.73	3.78	2.36	3.65	2.00	1.55	1.59	4.31	3.10	3.77	3.79	1.90	0.61	5.07	4.97	5.33	4.27	4.80	4.16	4.30	3.82	4.25
RSD, %	*10.3*	*1.1*	*3.6*	*6.2*	*8.7*	*13.1*	*8.5*	*0.6*	*3.8*	*1.1*	*5.7*	*3.4*	*1.5*	*10.4*	*6.6*	*2.5*	*1.9*	*4.0*	*2.8*	*2.6*	*5.8*	*3.5*	*6.4*	*1.9*	*3.0*
Major elements (in wt%) by EMPA (CSL, UTAS)																									
SiO_2	47.43	46.59	45.62	46.36	44.54	45.84		47.83	47.32	49.40	46.33		45.05	46.27	45.77	46.34	48.34	48.62	47.95	47.68	47.49	47.52	48.78	47.49	45.99
TiO_2	1.35	1.17	1.13	0.80	0.74	1.00		1.73	1.32	1.82	1.06		1.15	0.90	1.13	1.06	0.81	1.05	0.96	1.03	0.85	0.92	0.82	0.90	0.85
Al_2O_3	15.92	16.05	15.19	13.03	10.32	13.93		14.06	14.88	14.90	14.14		13.50	12.97	14.17	15.98	13.73	14.71	13.13	13.92	13.98	13.63	13.31	14.05	12.54
FeO	7.14	6.55	7.74	7.18	12.23	8.44		9.48	9.21	8.51	6.88		8.90	8.66	7.03	7.69	7.42	7.69	8.40	8.18	6.98	8.50	8.05	8.64	7.08
MnO	0.11	0.10	0.13	0.13	0.19	0.14		0.16	0.14	0.13	0.12		0.15	0.12	0.13	0.09	0.15	0.15	0.14	0.14	0.13	0.17	0.14	0.16	0.13
MgO	6.77	6.98	7.42	8.77	9.11	8.39		7.43	7.21	6.55	8.01		7.36	7.76	6.55	7.21	7.89	3.87	7.63	6.50	7.29	7.86	7.37	6.90	7.43
CaO	11.74	14.28	13.87	14.44	12.81	13.08		9.57	10.74	8.78	12.78		13.94	12.44	15.43	14.10	12.62	13.74	12.12	13.35	13.81	12.45	12.84	13.37	13.57
Na_2O	2.92	2.42	2.57	1.68	1.61	2.24		2.75	2.70	3.08	2.22		1.68	2.11	1.73	2.94	2.25	2.37	2.21	2.27	2.06	2.27	2.07	2.42	1.85
K_2O	1.20	0.76	0.83	0.88	0.54	0.75		1.43	1.32	2.12	0.70		0.64	0.71	0.80	0.80	0.50	0.76	0.55	0.66	1.05	0.70	0.62	0.70	0.83
P_2O_5	n.a.	n.a.	n.a.	n.a.	n.a.	n.a.		n.a.	n.a.	n.a.	n.a.		n.a.	n.a.	n.a.	n.a.	0.19	0.23	0.17	0.26	0.16	0.25	0.15	0.16	0.18
SO_3	0.40	0.48	0.54	0.45	0.44	0.51		0.26	0.38	0.15	0.53		0.33	0.58	0.57	0.20	0.59	0.77	0.67	0.74	0.57	0.61	0.68	0.65	0.56
Cl	0.09	0.13	0.13	0.07	0.09	0.11		0.07	0.10	0.06	0.10		0.08	0.09	0.12	0.12	0.11	0.13	0.11	0.11	0.09	0.11	0.10	0.10	0.12
F	0.03	0.06	0.05	0.03	0.04	0.03		0.03	0.04	0.02	0.03		0.04	0.03	0.00	0.04	n.a.	n.a.	n.a.	n.a.	n.a.	n.a.	n.a.	n.a.	n.a.
Total	95.10	95.60	95.22	93.82	92.65	94.46		94.81	95.39	95.51	92.90		92.80	92.66	93.42	96.57	94.60	94.09	94.05	94.84	94.44	95.00	94.93	95.52	91.12
Host olivine Fo, mol%	87.9	90.2	89.1	90.7	86.4	89.2		83.6	84.8	84.6	90.1		88.7	88.3	91.0	88.2	91.0	88.2	88.2	88.5	90.9	88.2	88.5	88.5	91.0

N repl - number of replicated analyses and number of accepted analyses of CO_2 in parentheses; D – diameter of melt inclusions and vapor bubbles; RSD - relative standard deviation external reproducibility of the same melt inclusion calculated from three measurements, and is equal to internal uncertainty in the case of 1 measurement; n.a. - not analyzed.

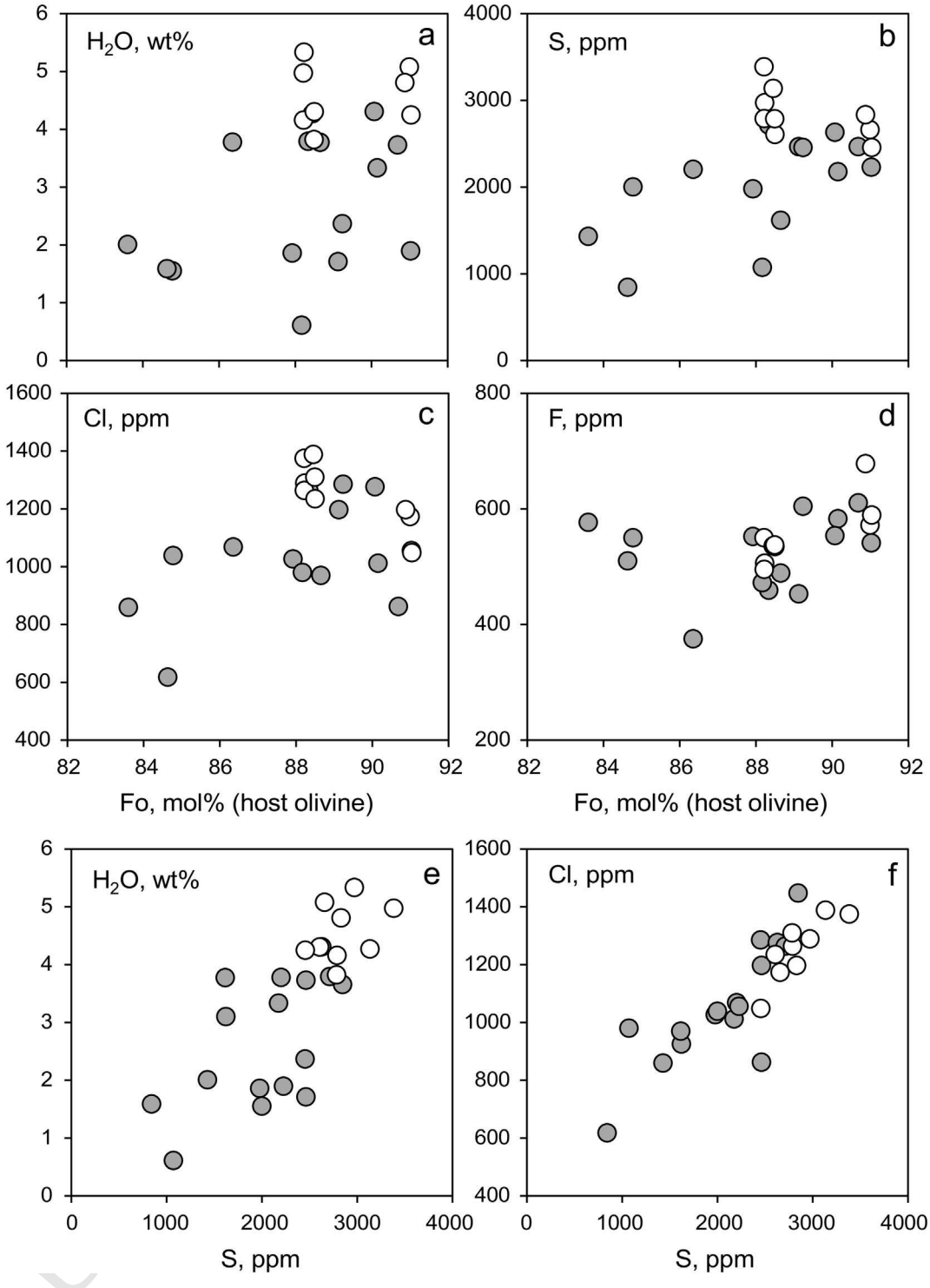

Fig. 11. Relationships between abundances of volatile elements in melt inclusions and host olivine Fo content (a-d) and sulfur content and other volatile elements (e, f). Melt inclusions are naturally glassy (GMI, *open circles*) and initially crystalline and then homogenized (CMI, *filled circles*).

The existence of melts with high CaO/Al_2O_3 compositions is unequivocal in the case of olivine-hosted melt inclusions, including those reported in this study, but this then presents a dilemma as to their origin. Peridotite melting experiments (e.g. Falloon et al., 1989; Jaques and Green, 1980) showed that CaO/Al_2O_3 rise with progressive partial melting from values initially below that of the mantle source composition (i.e. 0.8) until they marginally exceed the source value at the point of clinopyroxene exhaustion. The CaO/Al_2O_3 values of the melt inclusions correlate neither with trace-element parameters that could be anticipated to vary with degree of melting nor with other major-element variables that are known to depend on extent of peridotite melting. Nonetheless, the experimental melt compositions with lherzolite or harzburgite residues do not approach or reach those of the studied melt inclusions.

Several possible explanations have been proposed to account for the normative diopside-rich compositions of primitive melt inclusions in several island-arc volcanic suites. One possible scenario may involve melting of a clinopyroxene-rich source material, such as a wehrlitic

Please cite this article as: Kamenetsky, V.S., et al., Reprint of Silicate-sulfide liquid immiscibility in modern arc basalt (Tolbachik volcano, Kamchatka): Part II. Composition, liquidus assemblage and ..., Chem. Geol. (2017), https://doi.org/10.1016/j.chemgeo.2017.10.026

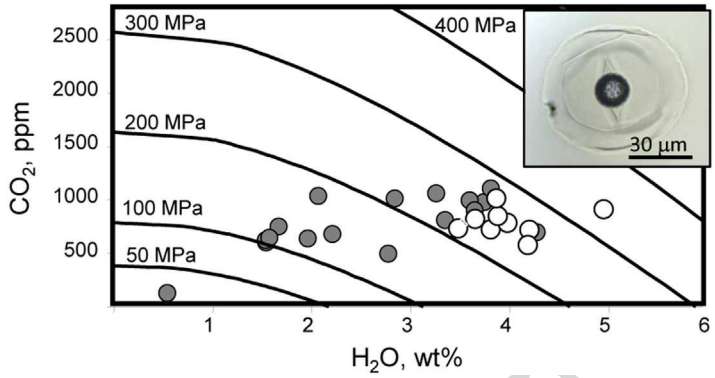

Fig. 12. Relationships between H_2O and CO_2 contents in melt inclusions. Isobars are calculated using VolatileCalc (Newman and Lowenstern, 2002) at 1220 °C and 47.5 wt% SiO_2 in melt. Inset shows typical glassy silicate melt inclusion in 1941 Tolbachik olivine with CO_2-rich vapor bubble, containing carbonate and sulfate precipitates on the walls. Melt inclusions are naturally glassy (GMI, *open circles*) and initially crystalline and then homogenized (CMI, *filled circles*).

mantle source or clinopyroxene-rich veins or layers in the mantle (Kamenetsky et al., 1997). However, the Tolbachik magmas have been assigned a purely peridotite source (Portnyagin et al., 2015) based on their CaO–MgO systematics (>13.81–0.247 * MgO (Herzberg and Asimow, 2008) and Ni and Mn contents in primitive olivine (NiO <0.4% and FeO/MnO <70; Herzberg, 2011; Sobolev et al., 2007). This conclusion is fully confirmed by our data on the 1941 Tolbachik melt inclusions (Fig. 8) and their host olivine compositions (Figs. 4, 5).

An alternative to unconventional mantle lithologies, such as wehrlite and pyroxenite, in the origin of high-Ca melts has been proposed as the concept of localized processes of dissolution, reaction and mixing (DRM) in the magmatic plumbing system and successfully applied in interpretation of compositionally anomalous melt inclusions (Danyushevsky et al., 2004). Significant increase in CaO/Al_2O_3 ratios of mantle-derived melts due to interactions with wall rocks has been strongly advocated in recent experimental studies (e.g. Mitchell and Grove, 2016). Locally contaminated melts are prone to aggregation prior to eruption, and thus the effects of contamination in the erupted magmas can be gradually obliterated by magma mixing and masked by crystal fractionation.

5.4. Initial volatile contents

Highly variable concentrations of volatile components in melt inclusions (Figs. 11–13) suggest that more than one competing process governed their concentrations. These processes include diffusive loss of volatiles from melt inclusions, redistribution of volatiles between residual melt and fluid phase in inclusions, crystallization, magma degassing and mixing.

Experimental and theoretical modelling has shown that hydrogen dissipates rapidly from melt inclusions, especially at high temperature (>1000 °C), and the concentration of H_2O in melt inclusions is susceptible to changes after entrapment (e.g. Chen et al., 2011; Gaetani et al., 2012; Massare et al., 2002; Mironov et al., 2015; Portnyagin et al., 2008; Sobolev and Chaussidon, 1996). It is also experimentally established that high-H_2O melt inclusions are particularly susceptible to diffusive dehydration (Gaetani et al., 2012), and they may lose significant amount of H_2O during homogenization at ambient pressure (Massare et al., 2002). Several studies of natural systems have advised that hydrogen can diffuse into or from melt inclusions to achieve equilibrium with the external melt (Danyushevsky et al.,

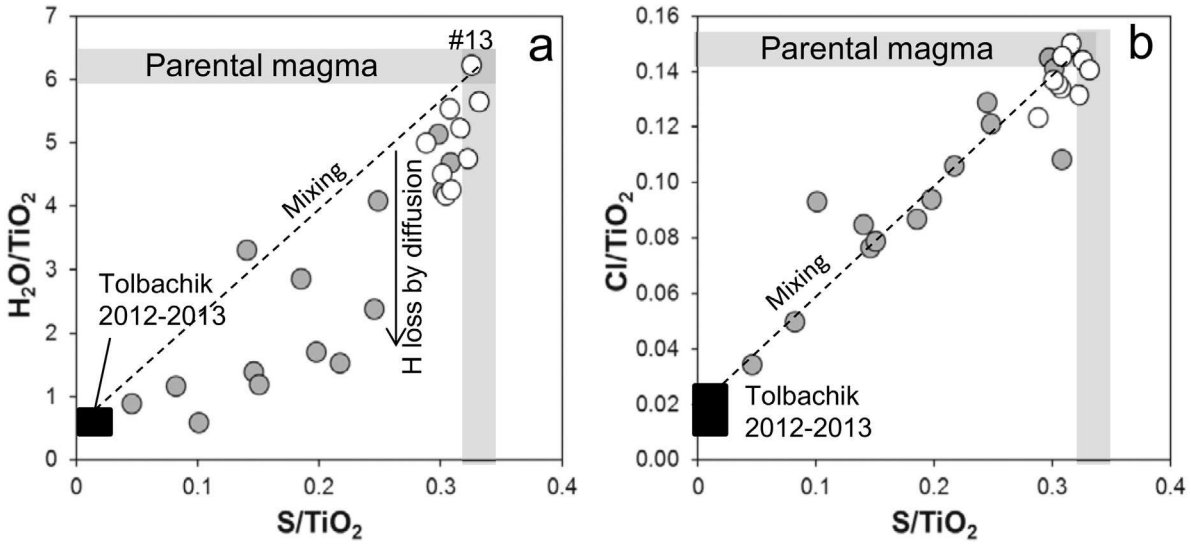

Fig. 13. Systematics of volatiles in the Tolbachik melt inclusions. Volatile concentrations are normalized to TiO_2 content to eliminate effects of crystallization. All concentrations are in wt%. The highest Ti-normalized volatile concentrations were measured by SIMS in naturally quenched melt inclusion #13 in olivine Fo_{91} ($H_2O/TiO_2 = 6.2$, $S/TiO_2 = 0.33$, $Cl/TiO_2 = 0.14$), which also has the largest size (~150 mm) of all inclusions studied. Volatiles in inclusion #13 are thought to represent those in parental Tolbachik magmas. Concentrations of volatiles in other inclusions are variably affected by 1) diffusive H loss from inclusions, 2) mixing with evolved magmas, and 3) magma degassing (see text for discussion). Evolved Tolbachik magmas are exemplified by the composition of inclusions in olivine Fo_{72-76} from the 2012–2013 Tolbachik eruption (Plechov et al., 2015). Melt inclusions are naturally glassy (GMI, *open circles*) and initially crystalline and then homogenized (CMI, *filled circles*).

Please cite this article as: Kamenetsky, V.S., et al., Reprint of Silicate-sulfide liquid immiscibility in modern arc basalt (Tolbachik volcano, Kamchatka): Part II. Composition, liquidus assemblage and ..., Chem. Geol. (2017), https://doi.org/10.1016/j.chemgeo.2017.10.026

2002; Kamenetsky et al., 1998; Mironov et al., 2015; Portnyagin et al., 2008; Sobolev, 1996).

In the case of Tolbachik, H_2O in melt inclusions exhibit strong variability at a given Fo content of the host olivine (Fig. 11a) that can be attributed to irregular hydrogen loss from inclusions as described above. The H_2O loss is particularly evident for initially crystalline and then reheated inclusions (CMI; Figs. 11a, 13a). Apparently, such inclusions can lose H_2O during slow cooling in lava and also in homogenization experiments (e.g. Chen et al., 2011; Lloyd et al., 2013). H_2O content in naturally quenched GMI in olivine from scoria are systematically higher and should be more informative of the initial H_2O values. Thus, deeper crystallization, fast evacuation and related quenching of the GMI-hosting olivine crystals appear to be plausible explanations for H_2O-rich compositions and glassy appearance of the melt inclusions.

The highest H_2O/TiO_2 was determined for the largest GMI in olivine Fo_{91} (#13, Table 2, Fig. 13a). TiO_2 is chosen here as denominator because it is routinely analyzed, behaves incompatibly in most basaltic melts prior to crystallization of Ti-magnetite and ilmenite, and does not depend, as strongly as more incompatible elements (e.g. K, Ce), on melting degrees and melt/fluid contributions from subducted slabs. By using the highest $H_2O/TiO_2 = 6.2$ as representative for parental Tolbachik melts, their initial H_2O content is estimated in four melt inclusions trapped in Fo_{91} as high as 4.7–5.2 wt% (average 4.9 wt%, Supplementary Table S5). The H_2O content exceeds significantly previous estimates made using experimentally homogenized inclusions in Tolbachik olivine (2.4–2.8 wt%, Portnyagin et al., 2007) but agrees well with the new model estimates (Portnyagin et al., 2015) and also with H_2O content in inclusions from neighboring Klyuchevskoy volcano, which were completely homogenized under high H_2O pressure and argued to represent initially trapped compositions (4–5 wt% H_2O, Mironov et al., 2015).

H_2O, sulfur, chlorine and fluorine, as well as their Ti-normalized concentrations in the Tolbachik inclusions are all positively correlated (Figs. 11, 13). The most H_2O rich inclusions in olivine Fo_{91} have also the highest S/TiO_2 (~0.33) and Cl/TiO_2 (~0.14), thus denoting parental melt compositions with the initial S = 2480–2760 ppm (average 2630 ppm) and Cl = 1090–1210 ppm (average 1160 ppm). Notably, the estimated sulfur contents in parental Tolbachik melts are close to the experimentally determined sulfur concentrations at sulfide saturation (SCSS) at ΔQFM ~1–1.5, 1 GPa and 1300 °C (1820–3090 ppm assuming the amount of S^{-2} in melt of 1200 ppm according to equation #7 in Jugo, 2009). Thus the melts could indeed be parental for immiscible sulfide associated with melt inclusions in the 1941 Tolbachik olivine.

Decreasing S and Cl contents with decreasing H_2O might reflect coupled loss of these volatiles from melt inclusions. However, diffusivity of S and Cl in olivine appears to be very slow and cannot occur on the same time scales as hydrogen diffusion (e.g. Bucholz et al., 2013; Portnyagin et al., 2008). Bucholz et al. (2013) have proposed that dehydration of melt inclusions can cause redistribution of S from melt to fluid bubble. The documented magnitude of this effect (~20–30%) is, however, much smaller compared to 3-fold variations of sulfur in Tolbachik melt inclusions and can hardly explain correlation of H_2O, S and Cl in glasses. Possible explanation for these covariations may be mixing of primitive and evolved melts under Tolbachik volcanic field. Plechov et al. (2015) documented evolved melt inclusions in olivine from the 2012–2013 eruption that contain ~1.2 wt% H_2O, ~300 ppm S and ~500 ppm Cl. Mixing of primitive Tolbachik magmas with evolved melts similar to those from the 2012–2013 eruption (Fig. 13) can readily explain much variability observed in the inclusions from 1941 eruption, in particular strong correlation between S and Cl, generally not expected from shallow magma degassing (e.g. Lesne et al., 2011).

Concentrations of CO_2 in melt inclusions (<1200 ppm) are comparable to those measured in naturally quenched and reheated at 1 atm melt inclusions from the Klyuchevskoy volcano (Auer et al., 2009; Mironov and Portnyagin, 2011). All melt inclusions studied here contain fluid bubble occupying up to 6% by volume, which stores likely a large fraction of CO_2 initially dissolved in trapped melt. The original CO_2 content of natural melts and those trapped as inclusions in olivine was undoubtedly higher than measured in the melt inclusions (<1200 ppm, Fig. 12, Table 2), because 40–90% (average 75%) of the original CO_2 dissolved in the melt at the time of inclusion entrapment can be lost to the shrinkage bubble during post-entrapment cooling (e.g. Mironov et al., 2015; Moore et al., 2015; Wallace et al., 2015).

5.5. Temperature and pressure of crystallization

The Petrolog3 algorithm (Danyushevsky and Plechov, 2011) and experimental data on the effect of H_2O on olivine liquidus (Almeev et al., 2007) were applied to the studied melt inclusions to calculate compositions and temperatures of the 1941 Tolbachik melts crystallizing olivine and undergoing sulfide immiscibility. The modelling demonstrates that the hydrous (ca. 5 wt% H_2O used in calculation) melt in equilibrium with olivine Fo_{91} contains ~12 wt% MgO and has the temperature of 1200–1230 °C at 1 GPa (Supplementary Table S5). These estimates are consistent with temperatures of 1139 to 1189 °C for host olivine $Fo_{89.9–89.3}$ estimated by Al-in-olivine thermometry (Supplementary Table S3) and in close agreement with previous modelling of parental melts for the Tolbachik high-Mg, water-bearing (~4 wt% H_2O) basaltic series (Portnyagin et al., 2015; Portnyagin et al., 2007). The temperatures are ~100–120 °C lower than the crystallization temperatures of primitive oceanic magmas (e.g. Green et al., 2001; Kamenetsky, 1996). Such calculated temperatures support the notion that the mantle wedge temperature is below the dry peridotite solidus, and thus an addition of fluxing slab-derived components (e.g. aqueous fluid or hydrous melt) is required for melt generation (Portnyagin et al., 2015; Portnyagin et al., 2007).

The pressure of primitive olivine crystallization can be constrained based on measured abundances of H_2O and CO_2 in the melt inclusions (Table 2, Fig. 12) and available models of volatile element solubility in silicate melts (e.g. Newman and Lowenstern, 2002; Shishkina et al., 2010). The minimum crystallization pressure can be estimated as ca. 3 kbar on the basis of measured H_2O and CO_2 concentrations in glasses (Fig. 12). When CO_2 contents in the melt inclusions are corrected for losses to fluid bubbles, the pressure estimates can be realistically extended to 5–7 kbar or even higher if other dissolved volatiles (halogens and sulfur) are taken into account. Such high crystallization pressure conforms with the modelling of the olivine-clinopyroxene cotectic in the Tolbachik magmas (see Fig. 3 in Portnyagin et al., 2015) and imply beginning of Tolbachik magma crystallization at the lower crust conditions under central Kamchatka, where the total crustal thickness is estimated as 35 km (Levin et al., 2002).

5.6. Implications for silicate-sulfide immiscibility

We conclude that silicate-sulfide immiscibility (Fig. 2) in the primitive island-arc Tolbachik magma occurred at elevated pressure (>3 kbar) and high temperature (<1250 °C), prior to significant degassing of volatile components. The immiscibility was promoted by a moderately oxidized environment (deduced from the liquidus Cr-spinel composition), and substantially high S content of the melt. Although the measured S abundances in the least degassed (i.e. most H_2O-rich) are moderately elevated (Table 2), compared to those in other arc magmas (see review in Wallace and Edmonds, 2011), the presence of magmatic anhydrite in some crystalline melt inclusions (Fig. 3) alerts to locally anomalous concentrations of sulfur in the magmatic system. Importantly, occurrence, shape and size of anhydrite are suggestive of former Ca-sulfate liquid, immiscible and entrapped with both silicate and sulfide melts in crystallizing olivine (Fig. 3).

Anhydrite occurrences in arc magmas are not commonly reported, but those at the El Chichón and Pinatubo andesitic volcanoes are prominent and significant for understanding sulfur budgets during eruptions (Luhr, 2008; Luhr et al., 1984; Parat et al., 2011; Pasteris,

Please cite this article as: Kamenetsky, V.S., et al., Reprint of Silicate-sulfide liquid immiscibility in modern arc basalt (Tolbachik volcano, Kamchatka): Part II. Composition, liquidus assemblage and ..., Chem. Geol. (2017), https://doi.org/10.1016/j.chemgeo.2017.10.026

1996). Enrichment of some magmas in the anhydrite component remains controversial, but "*reaction with sulfur enriched material at some unknown depth beneath the volcano*" (Carroll and Rutherford, 1987), based on pyrite- and anhydrite-bearing lithic fragments in the 1982 El Chichón pumices, seems most plausible. Similarly, we envisage that lithospheric and crustal wall rocks encountered by upwelling magmas can be a significant source of local contamination by certain minerals/elements in the case of the Tolbachik volcano. This has been demonstrated by abundant occurrences of gold (abraded nuggets of hydrothermal origin, liquid droplets and crystals in volcanic sublimates) in products of the 1975 Tolbachik eruption (Zelenski et al., 2016). Hydrothermal activity, associated with waning stages of magma cooling, crystallization and degassing, is considered responsible for accumulations of sulfur (elemental, sulfate and sulfide) in and around the volcanic conduit. These are continuously reworked enriched by coupled dissolution and re-deposition in successive volcanic cycles, and thus can be the main source of anomalously high sulfur and metal budgets of the otherwise common magmas.

Thus, given a common association of anhydrite and Fe-Ni-Cu sulfide inclusions in the primitive 1941 Tolbachik olivine (Fig. 3), we propose local oversaturation of the silicate melt in sulfur to be chiefly responsible for the liquid unmixing. Our data show that sulfide immiscibility in arc magmas does not necessary require their reduced nature; high sulfur abundances in magmas allow to reach saturation with sulfide at QFM + 1 and higher.

Acknowledgements

We thank Karsten Goemann and Jay Thompson for high quality analytical data. Vladimir Naumov shared his melt inclusion database. The manuscript benefited from insightful reviews by Duane Smythe, Philipp Ruprecht and Maryjo Brounce. We also grateful to Kate Kiseeva and Klaus Mezger for comments and editorial handling. This is CRPG contribution #2537. This study was supported by the Russian Science Foundation grant #16-17-10145.

Appendix A. Supplementary data

Supplementary data to this article can be found online at http://dx.doi.org/10.1016/j.chemgeo.2017.10.026.

References

Ackermand, D., Hekinian, R., Stoffers, R., 2007. Mineralogy of magmatic sulfides and transition metal oxides from lavas of the Pitcairn hotspot and the Pacific Antarctic ridge. N. Jb. Mineral. (Abh.) 184, 77–94.

Almeev, R.R., Holtz, F., Koepke, J., Parat, P., Botcharnikov, R.E., 2007. The effect of H_2O on olivine crystallization in MORB: experimental calibration at 200 MPa. Am. Mineral. 92, 670–674.

Arculus, R.J., Johnson, R.W., 1981. Island-arc magma sources: a geochemical assessment of the roles of slab-derived components and crustal contamination. Geochem. J. 15, 109–133.

Ariskin, A.A., et al., 2013. Modeling solubility of Fe-Ni sulfides in basaltic magmas: the effect of nickel. Econ. Geol. 108, 1983–2003.

Auer, S.L., Bindeman, I., Wallace, P., Ponomareva, V.V., Portnyagin, M., 2009. The origin of hydrous, high-$\delta^{18}O$ voluminous volcanism: diverse oxygen isotope values and high magmatic water contents within the volcanic record of Klyuchevskoy volcano, Kamchatka, Russia. Contrib. Mineral. Petrol. 157, 209–230.

Ballhaus, C., Berry, R.F., Green, D.H., 1991. High pressure experimental calibration of the olivine-orthopyroxene-spinel oxygen geobarometer: implications for the oxidation state of the upper mantle. Contrib. Mineral. Petrol. 107, 27–40.

Barsdell, M., 1988. Petrology and petrogenesis of clinopyroxene-rich tholeiitic lavas, Merelava volcano, Vanuatu. J. Petrol. 29, 927–964.

Barsdell, M., Berry, R.F., 1990. Origin and evolution of primitive island arc ankaramites from western Epi, Vanuatu. J. Petrol. 31, 747–777.

Braitseva, O.A., et al., 1984. Holocene volcanism of the Tolbachik regional zone of cinder cones. In: Fedotov, S.A. (Ed.), The Great Tolbachik Fissure Eruption, Kamchatka, 1975–1976. Nauka, Moscow, pp. 177–209 (in Russian).

Brounce, M.N., Kelley, K.A., Cottrell, E., 2014. Variations in $Fe^{3+}/\Sigma Fe$ of Mariana arc basalts and mantle wedge fO_2. J. Petrol. 55, 2514–2536.

Bucholz, C.E., Gaetani, G.A., Behn, M.D., Shimizu, N., 2013. Post-entrapment modification of volatiles and oxygen fugacity in olivine-hosted melt inclusions. Earth Planet. Sci. Lett. 374, 145–155.

Canil, D., Fedortchouk, Y., 2000. Clinopyroxene-liquid partitioning for vanadium and the oxygen fugacity during formation of cratonic and oceanic mantle lithosphere. J. Geophys. Res. 105, 26003–26016.

Carroll, M.R., Rutherford, M.J., 1985. Sulfide and sulfate saturation in hydrous silicate melts. J. Geophys. Res. 90, 601–612.

Carroll, M.R., Rutherford, M.J., 1987. The stability of igneous anhydrite: experimental results and implications for sulfur behavior in the 1982 El Chichon trachyandesite and other evolved magmas. J. Petrol. 28, 781–801.

Chen, Y., Provost, A., Schiano, P., Cluzel, N., 2011. The rate of water loss from olivine-hosted melt inclusions. Contrib. Mineral. Petrol. 162, 625–636.

Churikova, T.G., Gordeychik, B.N., Edwards, B.R., Ponomareva, V.V., Zelenin, E.A., 2015a. The Tolbachik volcanic massif: a review of the petrology, volcanology and eruption history prior to the 2012–2013 eruption. J. Volcanol. Geotherm. Res. 307, 3–21.

Churikova, T.G., et al., 2015b. Petrological and geochemical evolution of the Tolbachik volcanic massif, Kamchatka, Russia. J. Volcanol. Geotherm. Res. 307, 156–181.

Danyushevsky, L.V., 2001. The effect of small amounts of H_2O on crystallisation of mid-ocean ridge and backarc basin magmas. J. Volcanol. Geotherm. Res. 110, 265–280.

Danyushevsky, L.V., Plechov, P., 2011. Petrolog3: integrated software for modeling crystallization processes. Geochem. Geophys. Geosyst. 12.

Danyushevsky, L.V., Della-Pasqua, F.N., Sokolov, S., 2000. Re-equilibration of melt inclusions trapped by magnesian olivine phenocrysts from subduction-related magmas: petrological implications. Contrib. Mineral. Petrol. 138, 68–83.

Danyushevsky, L.V., McNeill, A.W., Sobolev, A.V., 2002. Experimental and petrological studies of melt inclusions in phenocrysts from mantle-derived magmas: an overview of techniques, advantages and complications. Chem. Geol. 183, 5–24.

Danyushevsky, L.V., Leslie, R.A.J., Crawford, A.J., Durance, P., 2004. Melt inclusions in primitive olivine phenocrysts: the role of localized reaction processes in the origin of anomalous compositions. J. Petrol. 45, 2531–2553.

Della-Pasqua, F.N., Varne, R., 1997. Primitive ankaramitic magmas in volcanic arcs: a melt-inclusion approach. Can. Mineral. 35, 291–312.

Desborough, G.A., Anderson, A.T., Wright, T.L., 1968. Mineralogy of sulfides from certain Hawaiian basalts. Econ. Geol. 63, 636–644.

Elburg, M., Kamenetsky, V.S., Nikogosian, I., Foden, J., Sobolev, A.V., 2006. Coexisting high- and low-calcium melts identified by mineral and melt inclusion studies of a subduction-influenced syn-collisional magma from South Sulawesi, Indonesia. J. Petrol. 47, 2433–2462.

Elburg, M.A., Kamenetsky, V.S., Foden, J.D., Sobolev, A., 2007. The origin of medium-K ankaramitic arc magmas from Lombok (Sunda arc, Indonesia): mineral and melt inclusion evidence. Chem. Geol. 240, 260–279.

Ermakov, V.A., Vazheevskaya, A.A., 1973. Ostry and Plosky Tolbachik volcanoes. Bull. Volcanol. Station 49, 43–53 (in Russian).

Evans, K., Elburg, M.A., Kamenetsky, V.S., 2012. The oxidation state of sub-arc mantle. Geology 40, 783–786.

Falloon, T.J., Green, D.H., McCulloch, M.T., 1989. Petrogenesis of High-Mg and Associated Lavas from the North Tonga Trench. In: Crawford, A.J. (Ed.), Boninites. Unwin Hyman, London, pp. 357–395.

Flerov, G.B., Anan'ev, V.V., Ponomarev, G.P., 2015. The petrogenesis of rocks of the Ostryi and Ploskii volcanoes and the relationship between volcanic occurrences of basaltic and trachybasaltic magmas in the Tolbachik Dol area, Kamchatka. J. Volcanol. Seismol. 9, 162–181.

Foden, J., 1983. The petrology of calcalkaline lavas of Rindjani Volcano, east Sunda Arc: a model for island arc petrogenesis. J. Petrol. 24, 98–130.

Fonseca, R.O.C., Campbell, I.H., O'Neill, H.S.C., Fitzgerald, J.D., 2008. Oxygen solubility and speciation in sulphide-rich mattes. Geochim. Cosmochim. Acta 72, 2619–2635.

Francis, R.D., 1990. Sulfide globules in mid-ocean ridge basalts (MORB), and the effect of oxygen abundance in Fe-S-O liquids on the ability of those liquids to partition metals from MORB and komatiite magmas. Chem. Geol. 85, 199–213.

Gaetani, G.A., O'Leary, J.A., Shimizu, N., Bucholz, C.E., Newville, M., 2012. Rapid reequilibration of H_2O and oxygen fugacity in olivine-hosted melt inclusions. Geology 40, 915–918.

Gioncada, A., et al., 1998. A study of melt inclusions at Vulcano (Aeolian Islands, Italy): insights on the primitive magmas and on the volcanic feeding system. Bull. Volcanol. 60, 286–306.

Gordeev, E.I., et al., 2013. The Tolbachik fissure eruption of 2012–2013: preliminary results. Dokl. Earth Sci. 452, 1046–1050.

Green, D.H., Falloon, T.J., Eggins, S.M., Yaxley, G.M., 2001. Primary magmas and mantle temperatures. Eur. J. Mineral. 13, 437–451.

Gurenko, A.A., Poliakov, A.I., Kononkova, N.N., 1987. Immiscible sulfide segregations in minerals of early crystallization stages of basaltic rock series. 293. Dokl. Akad. Nauk SSSR, pp. 439–443.

Gurenko, A.A., Kamenetsky, V.S., Kerr, A., 2016. Oxygen isotopes and volatile contents of the Gorgona komatiites, Colombia: a confirmation of the deep mantle origin of H_2O. Earth Planet. Sci. Lett. 454, 154–165.

Hart, S.R., Dunn, T., 1993. Experimental cpx/melt partitioning of 24 trace elements. Contrib. Mineral. Petrol. 113, 1–8.

Haughton, D.R., Roeder, P.L., Skinner, B.J., 1974. Solubility of sulfur in mafic magmas. Econ. Geol. 69, 541–567.

Herzberg, C., 2011. Identification of source lithology in the Hawaiian and Canary Islands: implications for origins. J. Petrol. 52, 113–146.

Herzberg, C., Asimow, P.D., 2008. Petrology of some oceanic island basalts: PRIMELT2.XLS software for primary magma calculation. Geochem. Geophys. Geosyst. 9.

de Hoog, J.C.M., Mason, P.R.D., van Bergen, M.J., 2001. Sulfur and chalcophile elements in subduction zones: constraints from a laser ablation ICP-MS study of melt inclusions from Galunggung Volcano, Indonesia. Geochim. Cosmochim. Acta 65, 3147–3164.

Jaques, A.L., Green, D.H., 1980. Anhydrous melting of peridotite at 0–15 kb pressure and the genesis of tholeiitic basalts. Contrib. Mineral. Petrol. 73, 287–310.

Please cite this article as: Kamenetsky, V.S., et al., Reprint of Silicate-sulfide liquid immiscibility in modern arc basalt (Tolbachik volcano, Kamchatka): Part II. Composition, liquidus assemblage and ..., Chem. Geol. (2017), https://doi.org/10.1016/j.chemgeo.2017.10.026

Jugo, P.J., 2009. Sulfur content at sulfide saturation in oxidized magmas. Geology 37, 415–418.

Kamenetsky, V., 1996. Methodology for the study of melt inclusions in Cr-spinel, and implications for parental melts of MORB from FAMOUS area. Earth Planet. Sci. Lett. 142, 479–486.

Kamenetsky, V.S., Eggins, S.M., 2012. Systematics of metals, metalloids, and volatiles in MORB melts: effects of partial melting, crystal fractionation and degassing (a case study of Macquarie Island glasses). Chem. Geol. 302-303, 76–86.

Kamenetsky, V.S., Gurenko, A.A., 2007. Cryptic crustal contamination of MORB primitive melts recorded in olivine-hosted glass and mineral inclusions. Contrib. Mineral. Petrol. 153, 465–481.

Kamenetsky, V.S., Kamenetsky, M.B., 2010. Magmatic fluids immiscible with silicate melts: examples from inclusions in phenocrysts and glasses, and implications for magma evolution and metal transport. Geofluids 10, 293–311.

Kamenetsky, V., Métrich, N., Cioni, R., 1995a. Potassic primary melts of Vulsini (Roman Province): evidence from mineralogy and melt inclusions. Contrib. Mineral. Petrol. 120, 186–196.

Kamenetsky, V.S., Sobolev, A.V., Joron, J.-L., Semet, M.P., 1995b. Petrology and geochemistry of Cretaceous ultramafic volcanics from East Kamchatka. J. Petrol. 36, 637–662.

Kamenetsky, V.S., Crawford, A.J., Eggins, S.M., Mühe, R., 1997. Phenocrysts and melt inclusion chemistry of near-axis seamounts, Valu Fa Ridge, Lau Basin: insight into mantle wedge melting and the addition of subduction components. Earth Planet. Sci. Lett. 151, 205–223.

Kamenetsky, V.S., et al., 1998. Calcic melt inclusions in primitive olivine at 43°N MAR: evidence for melt-rock reaction/melting involving clinopyroxene-rich lithologies during MORB generation. Earth Planet. Sci. Lett. 160, 115–132.

Kamenetsky, V.S., Crawford, A.J., Meffre, S., 2001. Factors controlling chemistry of magmatic spinel: an empirical study of associated olivine, Cr-spinel and melt inclusions from primitive rocks. J. Petrol. 42, 655–671.

Kamenetsky, V.S., Elburg, M., Arculus, R., Thomas, R., 2006. Magmatic origin of low-Ca olivine in subduction-related magmas: co-existence of contrasting magmas. Chem. Geol. 233, 346–357.

Kamenetsky, V.S., et al., 2007. Arrival of extremely volatile-rich high-Mg magmas changes explosivity of Mount Etna. Geology 35, 255–258.

Kamenetsky, V.S., et al., 2013. Noble metals potential of sulfide-saturated melts from the subcontinental lithosphere. Geology 41, 575–578.

Keith, J.D., et al., 1997. The role of magmatic sulfides and mafic alkaline magmas in the Bingham and Tintic mining districts, Utah. J. Petrol. 38, 1679–1690.

Kelley, K.A., Cottrell, E., 2009. Water and the oxidation state of subduction zone magmas. Science 325, 605–607.

Kelley, K.A., Cottrell, E., 2012. The influence of magmatic differentiation on the oxidation state of Fe in a basaltic arc magma. Earth Planet. Sci. Lett. 329, 109–121.

Kress, V.C., Carmichael, I.S.E., 1988. Stoichiometry of the iron oxidation reaction in silicate melts. Am. Mineral. 73, 1267–1274.

Larocque, A.C.L., Stimac, J.A., Keith, J.D., Huminicki, M.A.E., 2000. Evidence for open-system behavior in immiscible Fe-S-O liquids in silicate magmas: implications for contributions of metals and sulfur to ore-forming fluids. Can. Mineral. 38, 1233–1249.

Lee, C.T.A., Leeman, W.P., Canil, D., Li, Z.X.A., 2005. Similar V/Sc systematics in MORB and arc basalts: implications for the oxygen fugacities of their mantle source regions. J. Petrol. 46, 2313–2336.

Lee, C.T.A., Lee, T.C., Wu, C.T., 2014. Modeling the compositional evolution of recharging, evacuating, and fractionating (REFC) magma chambers: implications for differentiation of arc magmas. Geochim. Cosmochim. Acta 143, 8–22.

Lesne, P., et al., 2011. Experimental simulation of closed-system degassing in the system basalt-H_2O-CO_2-S-Cl. J. Petrol. 52, 1737–1762.

Levin, V., et al., 2002. Crust and upper mantle of Kamchatka from teleseismic receiver functions. Tectonophysics 358, 233–265.

Lloyd, A.C., Plank, T., Ruprecht, P., Hauri, E.H., Rose, W., 2013. Volatile loss from melt inclusions in pyroclasts of differing sizes. Contrib. Mineral. Petrol. 165, 129–153.

Luhr, J.F., 2008. Primary igneous anhydrite: progress since its recognition in the 1982 El Chichón trachyandesite. J. Volcanol. Geotherm. Res. 175, 394–407.

Luhr, J.F., Carmichael, I.S.E., Varekamp, J.C., 1984. The 1982 eruptions of El Chichon volcano, Chiapas, Mexico: mineralogy and petrology of the anhydrite-bearing pumices. J. Volcanol. Geotherm. Res. 23, 69–108.

Massare, D., Métrich, N., Clocchiatti, R., 2002. High-temperature experiments on silicate melt inclusions in olivine at 1 atm: inference on temperatures of homogenization and H2O concentrations. Chem. Geol. 183, 87–98.

Mathez, E.A., 1976. Sulfur solubility and magmatic sulfides in submarine basalt glass. J. Geophys. Res. 81, 4269–4276.

Mavrogenes, J.A., O'Neill, H.S.C., 1999. The relative effects of pressure, temperature and oxygen fugacity on the solubility of sulfide in mafic magmas. Geochim. Cosmochim. Acta 63, 1173–1180.

McCulloch, M.T., Gamble, J.A., 1991. Geochemical and geodynamical constraints on subduction zone magmatism. Earth Planet. Sci. Lett. 102, 358–374.

Melekestsev, I.V., Khrenov, A.P., Kozhemyaka, N.N., 1991. Tectonic position and general description of volcanoes of the Northern Group and Sredinny Range. In: Fedotov, S.A., Masurenkov, Y.P. (Eds.), Active Volcanoes of Kamchatka. Nauka, Moscow, pp. 74–81.

Métrich, N., Schiano, P., Clocchiatti, R., Maury, R.C., 1999. Transfer of sulfur in subduction settings: an example from Batan Island (Luzon volcanic arc, Philippines). Earth Planet. Sci. Lett. 167, 1–14.

Mironov, N.L., Portnyagin, M.V., 2011. H_2O and CO_2 in parental magmas of Kliuchevskoi volcano inferred from study of melt and fluid inclusions in olivine. Russ. Geol. Geophys. 52, 1353–1367.

Mironov, N., et al., 2015. Quantification of the CO_2 budget and H_2O–CO_2 systematics in subduction-zone magmas through the experimental hydration of melt inclusions in olivine at high H_2O pressure. Earth Planet. Sci. Lett. 425, 1–11.

Mitchell, A.L., Grove, T.L., 2016. Experiments on melt–rock reaction in the shallow mantle wedge. Contrib. Mineral. Petrol. 171.

Moore, L.R., et al., 2015. An assessment of the contribution of vapor bubbles to melt inclusion volatile budgets. Am. Mineral. 100, 806–823.

Naldrett, A.J., 1969. A portion of the system Fe-S-O between 900 and 1080 °C and its application to sulfide ore magmas. J. Petrol. 10, 171–201.

Naldrett, A.J., 2004. Magmatic Sulfide Deposits: Geology, Geochemistry and Exploration. Springer-Verlag, Berlin Heidelberg.

Newman, S., Lowenstern, J.B., 2002. VolatileCalc: a silicate melt-H_2O-CO_2 solution model written in visual basic for excel. Comput. Geosci. 28, 597–604.

O'Hara, M.J., 1977. Geochemical evolution during fractional crystallization of a periodically refilled magma chamber. Nature 266, 503–507.

O'Hara, M.J., Mathews, R.E., 1981. Geochemical evolution in an advancing, periodically replenished, periodically tapped, continuously fractionated magma chamber. J. Geol. Soc. Lond. 138, 237–277.

O'Neill, H.S.C., Mavrogenes, J.A., 2002. The sulfide capacity and the sulfur content at sulfide saturation of silicate melts at 1400 °C and 1 bar. J. Petrol. 43, 1049–1087.

Parat, F., Holtz, F., Streck, M.J., 2011. Sulfur-bearing magmatic accessory minerals. Rev. Mineral. Geochem. 285–314.

Pasteris, J.D., 1996. Mount Pinatubo volcano and "negative" porphyry copper deposits. Geology 24, 1075–1078.

Patten, C., Barnes, S.J., Mathez, E.A., 2012. Textural variations in MORB sulfide droplets due to differences in crystallization history. Can. Mineral. 50, 675–692.

Patten, C., Barnes, S.J., Mathez, E.A., Jenner, F.E., 2013. Partition coefficients of chalcophile elements between sulfide and silicate melts and the early crystallization history of sulfide liquid: LA-ICP-MS analysis of MORB sulfide droplets. Chem. Geol. 358, 170–188.

Perfit, M.R., Gust, D.A., Bence, A.E., Arculus, R.J., Taylor, S.R., 1980. Chemical characteristics of island-arc basalts: implications for mantle sources. Chem. Geol. 30, 227–256.

Piip, B.I., 1946. The activity of the Tolbachik volcano (January 1941). Bull. Volcanol. Station 12, 70–73 (In Russian).

Plechov, P., et al., 2015. Petrology and volatile content of magmas erupted from Tolbachik Volcano, Kamchatka, 2012–13. J. Volcanol. Geotherm. Res. 307, 182–199.

Portnyagin, M.V., Mironov, N.L., Matveev, S.V., Plechov, P.Y., 2005a. Petrology of avachites, high-magnesian basalts of Avachinsky volcano, Kamchatka: II. Melt inclusions in olivine. Petrology 13, 322–351.

Portnyagin, M.V., Plechov, P.Y., Matveev, S.V., Osipenko, A.B., Mironov, N.L., 2005b. Petrology of avachites, high-magnesian basalts of Avachinsky volcano, Kamchatka: I. General characteristics and composition of rocks and minerals. Petrology 13, 99–121.

Portnyagin, M., Hoernle, K., Plechov, P., Mironov, N., Khubunaya, S., 2007. Constraints on mantle melting and composition and nature of slab components in volcanic arcs from volatiles (H_2O, S, Cl, F) and trace elements in melt inclusions from the Kamchatka Arc. Earth Planet. Sci. Lett. 255, 53–69.

Portnyagin, M., Almeev, R., Matveev, S., Holtz, F., 2008. Experimental evidence for rapid water exchange between melt inclusions in olivine and host magma. Earth Planet. Sci. Lett. 272, 541–552.

Portnyagin, M., et al., 2015. Geochemistry of the late Holocene rocks from the Tolbachik volcanic field, Kamchatka: quantitative modelling of subduction-related open magmatic systems. J. Volcanol. Geotherm. Res. 307, 133–155.

Portnyagin, M.V., Mironov, N.L., Nazarova, D.P., 2017. Copper partitioning between olivine and melt inclusions and its content in primitive island-arc magmas of Kamchatka. Petrology 25, 419–432.

Ramsay, W.R.H., Crawford, A.J., Foden, J.D., 1984. Field setting, mineralogy, chemistry and genesis of arc picrites, New Georgia, Solomon Islands. Contrib. Mineral. Petrol. 88, 386–402.

Roedder, E., 1992. Fluid inclusion evidence for immiscibility in magmatic differentiation. Geochim. Cosmochim. Acta 56, 5–20.

Schiano, P., Eiler, J.M., Hutcheon, I.D., Stolper, E.M., 2000. Primitive CaO-rich, silica-undersaturated melts in island arcs: Evidence for the involvement of clinopyroxene-rich lithologies in the petrogenesis of arc magmas. Geochem. Geophys. Geosyst. 1 (Paper number 1999GC000032).

Schuth, S., et al., 2004. Geochemical constraints on the petrogenesis of arc picrites and basalts, New Georgia Group, Solomon Islands. Contrib. Mineral. Petrol. 148, 288–304.

Shishkina, T.A., Botcharnikov, R.E., Holtz, F., Almeev, R.R., Portnyagin, M.V., 2010. Solubility of H_2O- and CO_2-bearing fluids in tholeiitic basalts at pressures up to 500 MPa. Chem. Geol. 277, 115–125.

Skinner, B.J., Peck, D.L., 1969. An immiscible sulfide melt from Hawaii. Econ. Geol. Monogr. 4, 310–322.

Sobolev, A.V., 1996. Melt inclusions in minerals as a source of principle petrological information. Petrology 4, 228–239.

Sobolev, A.V., Chaussidon, M., 1996. H_2O concentrations in primary melts from supra-subduction zones and mid-ocean ridges: implications for H_2O storage and recycling in the mantle. Earth Planet. Sci. Lett. 137, 45–55.

Sobolev, A.V., Nikogosian, I.K., 1994. Petrology of long-lived mantle plume magmatism: Hawaii, Pacific and Reunion Island, Indian Ocean. Petrology 2, 111–144.

Sobolev, A.V., et al., 2007. The amount of recycled crust in sources of mantle-derived melts. Science 316, 412–417.

Sorbadere, F., Schiano, P., Métrich, N., 2013. Constraints on the origin of nepheline-normative primitive magmas in island arcs inferred from olivine-hosted melt inclusion compositions. J. Petrol. 54, 215–233.

Stone, W.E., Fleet, M.E., 1991. Nickel-copper sulfides from the 1959 eruption of Kilauea Volcano, Hawaii: contrasting compositions and phase relations in eruption pumice and Kilauea Iki lava lake. Am. Mineral. 76, 1363–1372.

Sun, S.-S., McDonough, W.F., 1989. Chemical and isotopic systematics of oceanic basalts: implications for mantle composition and processes. In: Saunders, A.D., Norry, M.J. (Eds.), Magmatism in the Ocean Basins. Geological Society Special Publication, London, pp. 313–345.

Wallace, P.J., Edmonds, M., 2011. The sulfur budget in magmas: evidence from melt inclusions, submarine glasses, and volcanic gas emissions. Rev. Mineral. Geochem. 215–246.

Wallace, P.J., Kamenetsky, V.S., Cervantes, P., 2015. Melt inclusion CO_2 contents, pressures of olivine crystallization, and the problem of shrinkage bubbles. Am. Mineral. 100, 787–794.

Wan, Z.H., Coogan, L.A., Canil, D., 2008. Experimental calibration of aluminum partitioning between olivine and spinel as a geothermometer. Am. Mineral. 93, 1142–1147.

Wilkinson, J.J., 2013. Triggers for the formation of porphyry ore deposits in magmatic arcs. Nat. Geosci. 6, 917–925.

Wohlgemuth-Ueberwasser, C.C., Fonseca, R.O.C., Ballhaus, C., Berndt, J., 2013. Sulfide oxidation as a process for the formation of copper-rich magmatic sulfides. Mineral. Deposita 48, 115–127.

Zelenski, M., Kamenetsky, V.S., Hedenquist, J., 2016. Gold recycling and enrichment beneath volcanoes: a case study of Tolbachik, Kamchatka. Earth Planet. Sci. Lett. 437, 35–46.

Zelenski, M., Kamenetsky, V.S., Mavrogenes, J.A., Danyushevsky, L.V., Matveev, D., Gurenko, A.A., 2017a. Platinum-group elements and gold in sulfide melts from modern arc basalt (Tolbachik volcano, Kamchatka). Lithos 290-291, 172–188.

Zelenski, M., Kamenetsky, V.S., Mavrogenes, J.A., Gurenko, A.A., Danyushevsky, L.V., 2017b. Silicate-sulfide liquid immiscibility in modern arc basalt (Tolbachik volcano, Kamchatka): Part I. Occurrence and compositions of sulfide melts. Chem. Geol. (this volume).

Please cite this article as: Kamenetsky, V.S., et al., Reprint of Silicate-sulfide liquid immiscibility in modern arc basalt (Tolbachik volcano, Kamchatka): Part II. Composition, liquidus assemblage and ..., Chem. Geol. (2017), https://doi.org/10.1016/j.chemgeo.2017.10.026